To the Graduate Council:

I am submitting herewith a dissertation written by Michael Pickelsimer entitled "Wireless Power Transfer with Power Factor Correction for Electric Vehicles." I have examined the final electronic copy of this dissertation for form and content and recommend that it be accepted in partial fulfillment of the requirements for the degree of Master of Science with a major in Electrical Engineering.

Leon M Tolbert
Major Professor

We have read this thesis and recommend its acceptance.

Leon M. Tolbert
Major Professor

Burak Ozpineci
Council Member

Fred Wang
Council Member

Accepted for the Council:

Carolyn R. Hodges

Vice Provost and

Dean of the Graduate School

(Original signatures are on file with official student records)

WIRELESS POWER TRANSFER SYSTEM WITH POWER FACTOR CORRECTION FOR ELECTRIC VEHICLES

A Thesis Presented for the
Master of Science
Degree
The University of Tennessee, Knoxville

Michael Christopher Pickelsimer
August 2012

Dedication

To my fiancée, Kristen Holdway,

for her love and dedication.

And to my parents,

Penny & Eathon Hicks and Chris & Sylvia Pickelsimer,

for their support and wisdom.

Acknowledgement

I would like to thank Dr. Leon Tolbert for his guidance and his willingness to provide insight on both academia and life in general. I would also like to thank Dr. David Irick, Dr. John Miller, Dr. Burak Ozpineci, and Dr. David Smith for allowing me the honor to work with them. Their wisdom inside and outside of the work place will never be forgotten. Additional thanks are extended to Dr. Fred Wang, Dr. Jeremy Holleman, and Dr. Jack Lawler for lending their knowledge and experience when requested.

This project would not have been possible were it not for Oak Ridge National Laboratory.

This work was supported in part by the Engineering Research Center Program of the National Science Foundation and the Department of Energy under NSF Award Number EEC-1041877 and the CURENT Industry Partnership Program.

Abstract

Wireless power transfer is currently a popular topic of research. Because there are no mechanical connections between the transmitter and receiver, power can be transferred whenever a system is within range of a transmitter. Coil-to-coil efficiencies of over 95% at multiple kW have been recorded by researchers, proving that this type of charger has the potential to be a viable charging solution. Electric vehicles are a primary target for this technology because wireless power transfer systems may be able to provide power both while the vehicle is stationary or while in motion.

Despite the promises of high efficiency and high power capabilities, wireless power transfer has significant hurdles to overcome before widespread adoption can occur. Research is currently directed into two distinct paths. One of the areas of interest is aimed at reducing the amount of reactive power demand from these systems to improve system efficiency, while the area of exploration is centered on finding ways to increase the range at which transfer is capable and finding ways to improve a system's resistance to misalignment.

This thesis outlines the physics behind the operation of wireless power transfer and describes some possible solutions to correct for the potential of poor power factor at the utility connection. For this to be completed, an

experimental wireless power transfer system in use by Oak Ridge National Laboratories will be used to validate a transfer system model for simulation purposes.

After the transfer model is analyzed, two examples of complete wireless power transfer systems for an electric vehicle will be modeled and simulated for discussion. The first model was created to prove that the selected power factor correction technique can correct for power factor at a range of operating conditions. A second model will be constructed and simulated to improve operating efficiencies of the system. Results from both models will then be compared.

Table of Contents

Chapter 1 Introduction 1

1.1 Electric Vehicle Overview 1

1.2 Wireless Power Transfer Introduction 6

1.3 Summary 7

Chapter 2 Problem Statement 9

2.1 Model Development 9

2.2 Coupling Coefficient's Effect on System Performance 13

2.3 Resistive Load's Effect on System Performance 18

2.4 Problem Statement Summary 23

Chapter 3 Literature Review 24

3.1 Introduction 24

3.2 Research to Increase WPT Coupling 24

3.3 Power Factor Correction 27

3.4 Literature Review Summary 28

Chapter 4 Wireless Power Transfer Simulations 29

4.1 Simulation Development 29

4.2 Receiver Controlled System Simulation 39

4.3 Transmitter Controlled System Simulation 45

4.4 Simulation Summary 52

Chapter 5 Conclusions and Recommendations 53

5.1 Conclusions 53

5.2 Recommendations 54

References 55

Vita..... 60

List of Figures

Figure 1.1: Series and parallel HEV configurations 3

Figure 1.2: Series-parallel configurations 5

Figure 2.1: Series-parallel wireless power transfer circuit. 9

Figure 2.2: Bode plots for the admittance of resonant circuits tuned to 22.6 kHz 11

Figure 2.3: Equivalent system model with transformer core. 12

Figure 2.4: Output power versus coupling coefficient and frequency. 15

Figure 2.5: Input reactive power versus coupling coefficient and frequency. 15

Figure 2.6: System efficiency versus coupling coefficient and frequency. 16

Figure 2.7: P_{in}, P_{out}, and Q_{in} versus frequency for a coupling coefficient of 0.15. 17

Figure 2.8: P_{in}, P_{out}, and Q_{in} versus frequency for a coupling coefficient of 0.3. 17

Figure 2.9: P_{in}, P_{out}, and Q_{in} versus frequency for a coupling coefficient of 0.4. 18

Figure 2.10: Output power versus load resistance and frequency. 19

Figure 2.11: Input reactive power versus load resistance and frequency. 19

Figure 2.12: Efficiency versus load resistance and frequency. 20

Figure 2.13: P_{in}, P_{out}, and Q_{in} versus frequency for a load resistance of 15 Ω. 21

Figure 2.14: P_{in}, P_{out}, and Q_{in} versus frequency for a load resistance of 30 Ω. 21

Figure 2.15: P_{in}, P_{out}, and Q_{in} versus frequency for a load resistance of 40 Ω. 22

Figure 3.1: DDQ-DD coil configuration 25

Figure 4.1: Receiver controlled system block diagram. 29

Figure 4.2: Series-parallel WPT simulated system. 30

Figure 4.3: Coils from the system which the simulated system is modeled. 30

Figure 4.4: Experimental results for WPT system at ORNL. 32

Figure 4.5: Simulated results of WPT system at ORNL. 33

Figure 4.6: Inverter model. 35

Figure 4.7: Non-inverting buck boost DC-DC converter. 36

Figure 4.8: Active rectifier. 37

Figure 4.9: Selected PFC rectifier. 38

Figure 4.10: Receiver controlled system without PFC (2kW test). 40

Figure 4.11: Receiver controlled model utility voltage and currents (2 kW test). 40

Figure 4.12: Receiver controlled model battery ripple current (2 kW test). 41

Figure 4.13: Receiver controlled system without PFC (4kW test). 42

Figure 4.14: Receiver controlled model utility voltage and currents (4 kW test). 43

Figure 4.15: Receiver controlled model battery ripple current (4 kW test). 43

Figure 4.16: Transmitter controlled system block diagram 46

Figure 4.17: Transmitter controlled system without PFC (2kW test). 47

Figure 4.18: Transmitter controlled model utility voltage and currents (2 kW test). 47

Figure 4.19: Transmitter controlled model battery ripple current (2 kW test). 48

Figure 4.20: Transmitter controlled system without PFC (4kW test). 49

Figure 4.21: Transmitter controlled model utility voltage and currents (4 kW test). 49

Figure 4.22: Transmitter controlled model battery ripple current (4 kW test). 50

List of Tables

Table 1: APEEM cost goals 2

Table 2: Equivalent circuit component values after considering coupling coefficient 12

Table 3: Component values of the simulated WPT system 14

Table 4: Critical impedances for various coupling coefficients 22

Table 5: Results from quasi-square input voltage testing 34

Table 6: Simulation results for the receiver controlled system 44

Table 7: Simulation results for the transmitter controlled system 51

Nomenclature

EMI	Electromagnetic interference
ESS	Energy storage system
EV	Electric vehicle
HEV	Hybrid electric vehicle
ICE	Internal combustion engine
ORNL	Oak Ridge National Laboratory
PFC	Power factor corrector
PHEV	Plug-in hybrid electric vehicle
THD	Total harmonic distortion
WPT	Wireless power transfer

C_1	Primary capacitor (transmitter)
C_2	Secondary capacitor (receiver)
I_{ripple}	Current ripple at the battery
k	Coupling coefficient
L_1	Primary inductor (transmitter)
L_{11}	Primary inductor including the effects of coupling coefficient
L_2	Secondary inductor (receiver)
L_{22}	Secondary inductor including the effects of coupling coefficient
M	Magnetizing inductance of the equivalent transformer
P_{in}	Input power (W)
P_{out}	Output power (W)
Q_0	Frequency at which the input reactive power is zero
Q_{in}	Input reactive power (VARs)
R_L	Load resistance
Z_C	Minimum impedance
Z_{CRIT}	Critical impedance

Chapter 1 Introduction

1.1 Electric Vehicle Overview

Automotive manufacturers are always trying to provide a vehicle that meets the needs and requests of consumers. Public opinion has dictated what research areas are of primary interest to the personal transportation industry. As of late, the public has been increasingly concerned with gas mileage due to increases in fuel prices and a growing concern with greenhouse gas emissions. One of the routes taken by the auto industry has been to introduce electric vehicles (EVs) and hybrid electric vehicles (HEVs).

Conventional vehicles are powered by an internal combustion engine (ICE). These vehicles are limited in efficiency because of thermodynamics and can achieve maximum efficiencies around 26% [1]. Electric machines are not limited by thermodynamic efficiency of combustion since they operate through electrical means. Electric machines can operate with efficiencies greater than 95%. However, since electric machines also require inverters and energy storage systems, which can operate with efficiencies as high as 95% and 80%, respectively. When all are combined, the electric drivetrain can operate with efficiencies near 70%.

Despite promises of high efficiency, EVs and HEVs suffer from other drawbacks. While the ICE found in a conventional vehicle has limitations on efficiency, it has been analyzed and improved upon by auto manufacturers for a significantly greater time than electric propulsion systems. Power electronics and traction drives are relatively new to the automotive market and have significant improvements yet to be made. A primary derivative of this issue is the increased cost of purchasing an EV/HEV. Additionally,

HEVs are typically much heavier than their conventional counterparts due the addition of the electric drive components, while Pure EVs have issues with the limited range from the lack of an ICE.

There are currently goals to reduce the cost of electrical components put in place by the Advanced Power Electronics and Electric Motors (APEEM) group within the U.S. Department of Energy [2]. The complete list of these goals can be seen in Table 1. Though the goals are directed at HEVs, advances are likely to carry over to the cost of EV components. Despite these goals, additional component requirements will have to be made to bring the cost of HEVs to a level that is comparable with a conventional counterpart. It is also important to note that these goals do not list battery costs.

As stated earlier, HEVs are heavier than their conventional counterparts. This is due mainly to the addition of power electronics, electric machines, and an energy storage system (ESS). One such comparison is the Toyota Camry Hybrid (3441 lbs.) and Toyota Camry (3190 lbs.) [3],[4]. Plug-in hybrid electric vehicles (PHEVs), a type of hybrid electric vehicle, contain a larger ESS than a traditional HEV to take advantage of the ability to charge the battery through grid connections. The exact components of HEVs vary with the system configuration. The three main configurations of HEV are series, parallel, and series-parallel [5],[6]. The energy flow diagrams of the series and parallel types can be seen in Figure 1.1.

Table 1: APEEM cost goals

Item ($/kW)	2010	2015	2020
Traction Drive System	19	12	8
Power Electronics	7.9	7	5
Motors	11.1	10	7

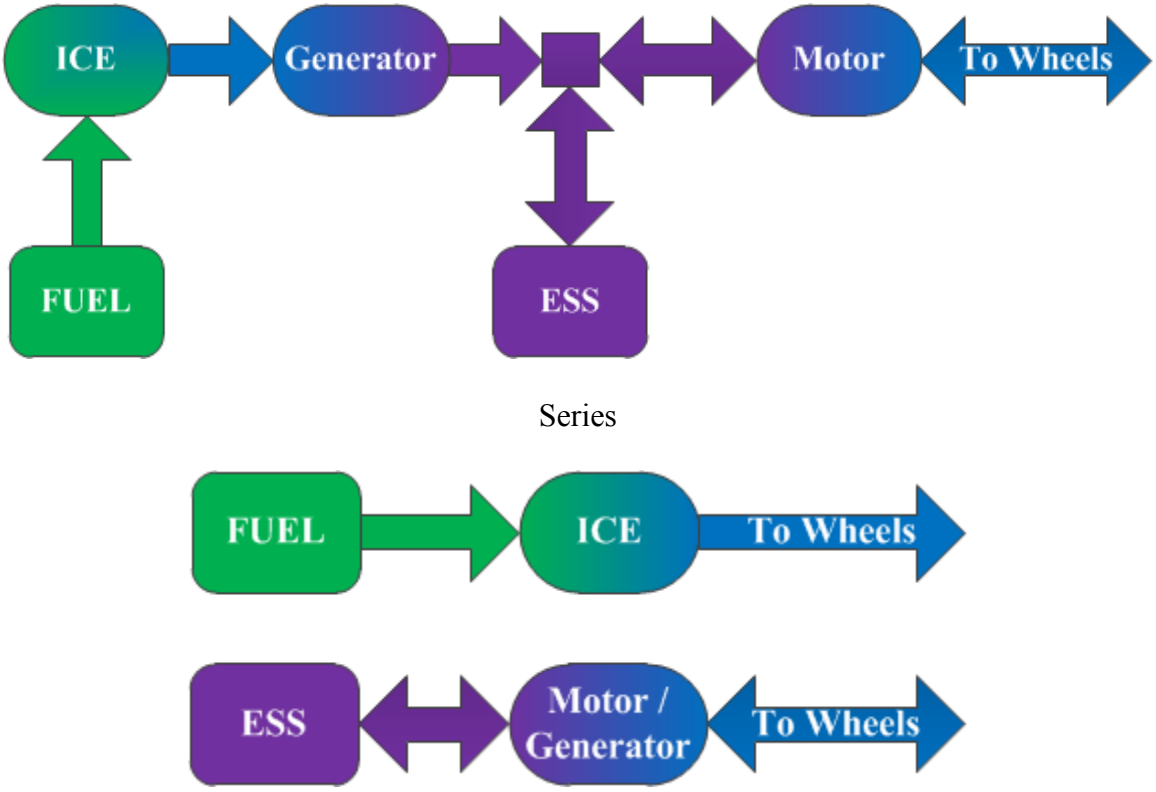


Figure 1.1: Series and parallel HEV configurations

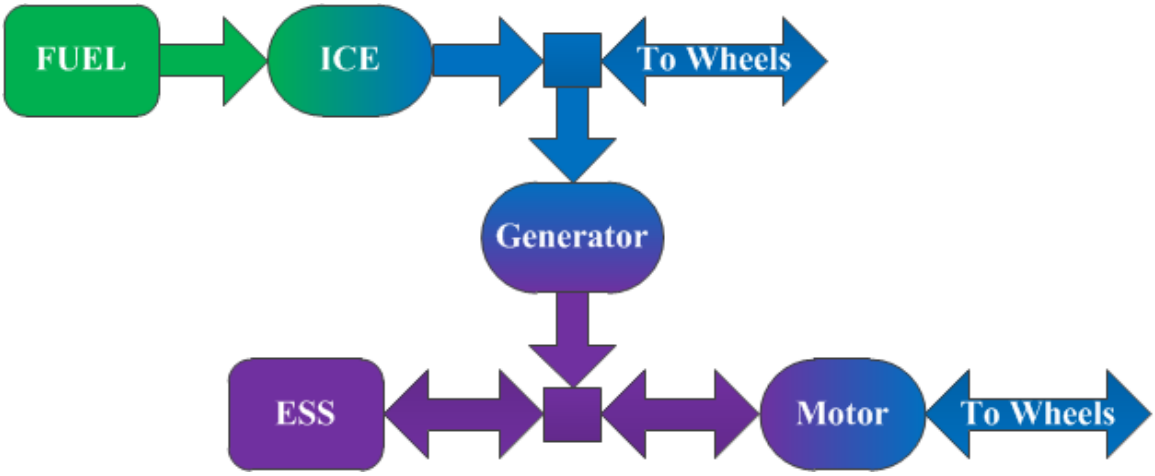
The series configuration has an electric generator mechanically linked to the ICE that provides electrical power to the energy storage system and the traction drive motor. This configuration allows the ICE to run at its most efficient operating point, but contains two electric machines capable of sourcing peak power from the ICE. As such, this configuration requires two large electric machines, a rectifier, and an inverter. Another disadvantage is the lack of redundancy in the drivetrain, which means that the vehicle cannot operate if there is an electrical problem.

Parallel HEVs, also called parallel through-the-road, is where the ICE is directly coupled to the road and the electric drivetrain is not directly linked to the ICE. The benefits of this drivetrain are that it provides the drivetrain redundancy missing in the

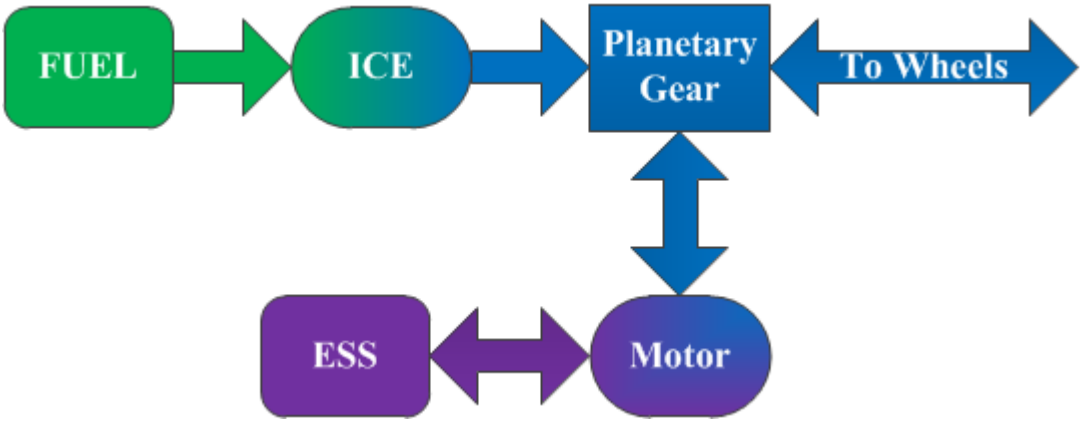
series configuration and it requires only a single electric machine and power converter. However, this system does not allow the ICE to charge the ESS if the vehicle is not moving.

A series-parallel HEV can be obtained by combining the two previously mentioned types. The ICE is coupled to an electric machine and a transmission. This can be done in two ways. The first way is to connect to the electric machine to the ICE drivetrain before or after the transmission. A clutch must be then added to allow the opportunity to disconnect the ICE from the road, while leaving connected to the electric machine. The electric machine is then connected components as it would be in a series configuration. When the clutch engaged the vehicle behaves as a series HEV. When the ICE drivetrain is coupled to the road, the vehicle can act as a parallel HEV. This architecture has two electric machines, an inverter, and a rectifier.

The second way that the series-parallel architecture can be obtained is through a planetary gear set that can be used to distribute power from the ICE to the road or electrical drivetrain independently, from the ICE to the road and electrical drivetrain simultaneously, or through the ICE and ESS to the road. This type of series-parallel architecture is referred to as a power split hybrid. While this has fewer components than the aforementioned series-parallel architecture (requiring only a single electric machine and converter) it contains the increased complexity of the planetary gear set. Despite this complex mechanical component, this type of HEV is very popular and can be found in the Toyota Prius [7]. The two series-parallel configurations can be seen in Figure 1.2.



Traditional Series-Parallel



Power Split

Figure 1.2: Series-parallel configurations

Pure EVs have limitations of their own. Because of their lack of an ICE, they are forced to contain a large ESS to provide the energy for the vehicle. When striving to increase the range of a vehicle, adding weight to said vehicle requires that it needs to expend more energy to move. When more energy is required to move per trip, more energy must be stored in the ESS. This compounding issue results in lower range, longer charge times, and higher cost of the vehicle to account for the increased energy content of the ESS.

In summary, EVs and HEVs have the potential to increase the efficiency of the transportation sector. However, they still have significant challenges to address before mass adoption can begin. Among these challenges are increased vehicle cost and increased vehicle mass.

1.2 Wireless Power Transfer Introduction

The problem of using a standard charger for EVs is that the vehicle has to physically plug into the power grid via a cable set. While this method is highly reliable, it does not provide the possibility of charging the ESS at during transit to and from a destination. Though EV chargers are becoming more prevalent in cities, they still require the driver to shut down the vehicle and physically plug the charger into a receptacle.

Wireless power transfer (WPT) may provide a partial solution to the range/mileage and cost problems for EVs and HEVs that does not require the driver to leave the vehicle to charge the battery. WPT, also called inductive power transfer or evanescent power transfer, may provide a relief from the large ESS necessary to increase EV range by allowing the vehicle to charge while in transit. Currently, research is being performed in stationary and in-motion WPT.

Stationary WPT chargers could be employed in most places where a current plug-in charger can be used, in addition to many places a plug-in charger cannot. WPT systems could be used at traffic signals and stop signs to provide momentary power supplies to charge a personal vehicle's ESS. Shuttles and public transportation that travel pre-determined routes could also take advantage of WPT chargers. The University of Tennessee, Chattanooga is currently doing work with electric busses to prove the usefulness of WPT in public transportation [8].

The ultimate goal of WPT meant for EVs and HEVs is in-motion activity. For example, a lane on a highway or interstate could be fitted with WPT chargers. EVs and HEVs passing over the chargers could be continuously charged, alleviating charge anxiety. Additionally, if a vehicle could be charged as it moves, it could employ a significantly smaller ESS. Reducing the size of the ESS can result in lower vehicle cost, shorter charge times, and overall improvements in vehicle range.

Unfortunately, WPT possesses its own challenges. Despite having high efficiencies, WPT has limited range and can operate with large reactive power components. While this poses a problem to the inverter providing power to the system, the utility cannot tolerate low power factors. As such, grid-side power factor correction must be addressed. Most research is being performed to increase the range and efficiency of WPT systems, leaving this problem with reactive power relatively uninvestigated.

1.3 Summary

This thesis will be used to investigate the potential to correct the displacement power factor at the utility connection and will compare two possible WPT systems. Before a possible solution is examined, however, the theory behind WPT will be reviewed in Chapter 2. Specific interest will be placed on the effects of coupling coefficient between the transmitter and receiver and the effects of load characteristics. Chapter 3 will be used to highlight a small portion of the research being performed to improve the operation of WPT. The research discussed will be separated into two topics: increasing the coupling coefficient and reducing reactive power demands. After the literature review, two models that describe possible WPT systems will be simulated and

compared in Chapter 4. Finally, Chapter 5 will be used to summarize the work performed, draw conclusions, and make recommendations.

Chapter 2 Problem Statement

2.1 Model Development

Some amount of wireless power transfer is possible wherever an electromagnetic field is present. Most electrical power transferred without the assistance of low resistance wires or highly magnetic materials is inefficient and typically unwanted. One of the most common types of wireless power transfer that fits this description is unintended magnetic coupling between inductors via an air gap. A second example of unwarranted wireless power transfer is an equivalent capacitor that causes unintended grounding, which contributes to electromagnetic interference (EMI).

For the purposes of this thesis WPT is the transfer of power over an air gap based on coupled magnetic coils in resonant circuits. When two circuits are tuned to be resonant at the same frequency, there can be a highly efficient transfer of power. The most common resonant transfer circuit consists of a series tuned transmitting circuit and a parallel tuned receiving circuit (series-parallel), such as the one shown in Figure 2.1. This model will be the basis of further discussion because of its simplicity and widespread usage.

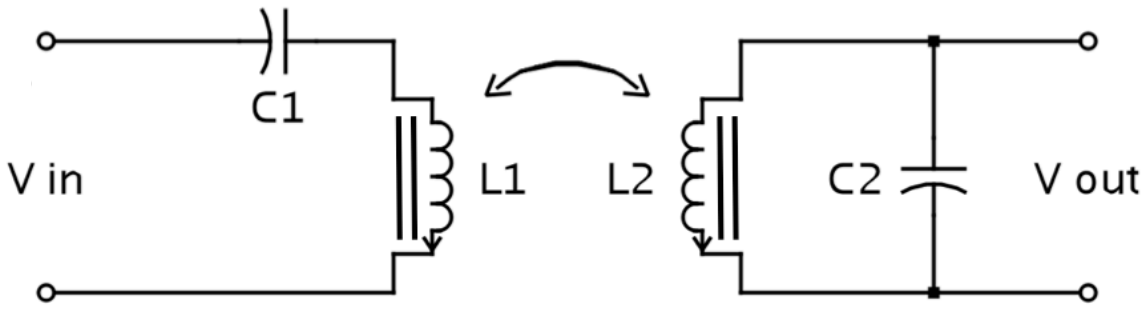
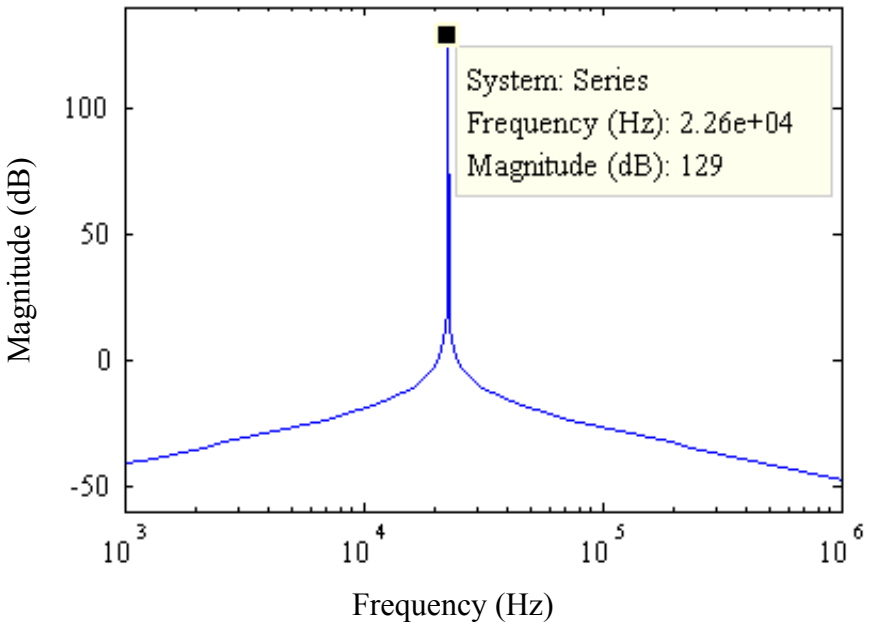


Figure 2.1: Series-parallel wireless power transfer circuit.

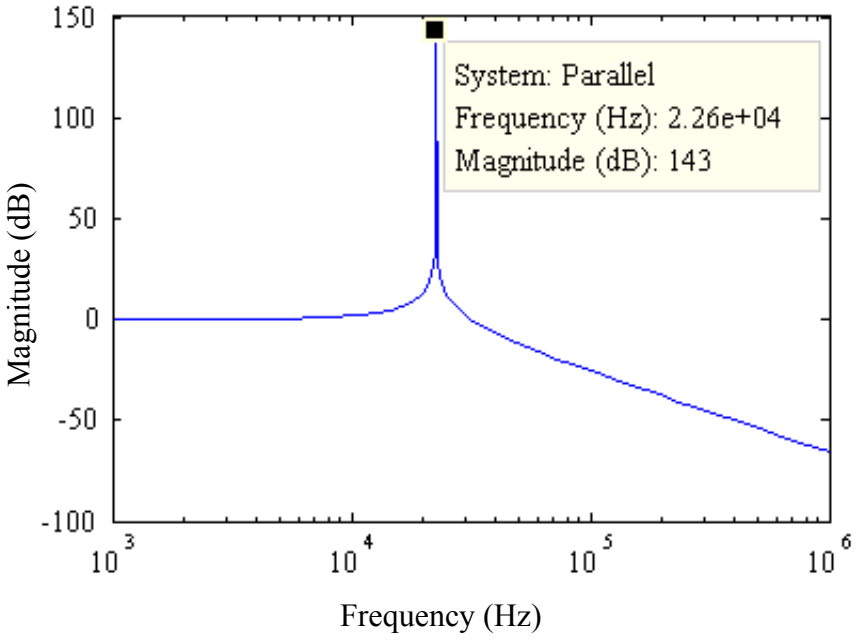
Highly efficient power transfer is possible because of the large magnetic field that can be created within the inductors of the transmitting circuit. When operated at resonance, the impedance of the system is reduced to a minimum level. A low level of impedance leads to a higher current within the system. This leads to a power magnetic flux generated by the transmitter. The receiving coil is excited by the magnetic flux from the positive coil, generating a voltage across the inductor. Since the voltage generated has the same frequency as is resonant in the receiver, the reactance of the receiving circuit is minimized, leaving only the load.

The transmitting circuit of the system, consisting of a series connected capacitor and inductor, acts as a bandpass circuit. This circuit allows only a limited band of frequencies to pass, while the rest are attenuated as the operational frequency moves further from the resonant point. The receiving circuit acts as a low pass filter that reduces the effects of high frequency while allowing lower frequencies to pass through with lower attenuation. However, this low pass circuit has been designed with a low coefficient of dampening that creates a large resonant frequency.

Differences in the resonant frequency can have negative impacts on the amount of power that can be transferred between the circuits because of the attenuation found in either circuit. Similarly, as the operating frequency moves further away from the resonant point of the complete system, a limited amount of power can still be transferred if the transmitter and receiver are tuned to similar resonant points. Examples of the spectra of the impedance of series-parallel tuned transmitting and receiving circuits that are tuned to 22.6 kHz can be found in Figure 2.2.



(a)



(b)

Figure 2.2: Bode plots for the admittance of resonant circuits tuned to 22.6 kHz in a series configuration (a) and a parallel configuration (b).

Because the WPT circuits are tuned to specific frequencies, they act as resonant converters with the magnetic material used as the core of the transformer removed. The equivalent circuit model of the transformer (found inserted into the series-parallel system in Figure 2.3) is preserved, though removing the core of the transformer results in a dramatically reduced coupling coefficient between the inductors. The modified component values that account for the effects of coupling coefficient, k, for the system can be seen in Table 2.

Since the coils form a magnetic coupling, the coupling coefficient between the transmitter and receiver is inversely linked to the vertical distance between the transmitting and receiving coils. Other factors that contribute to the coupling coefficient are angular and lateral displacement and the presence of magnetic field shaping components.

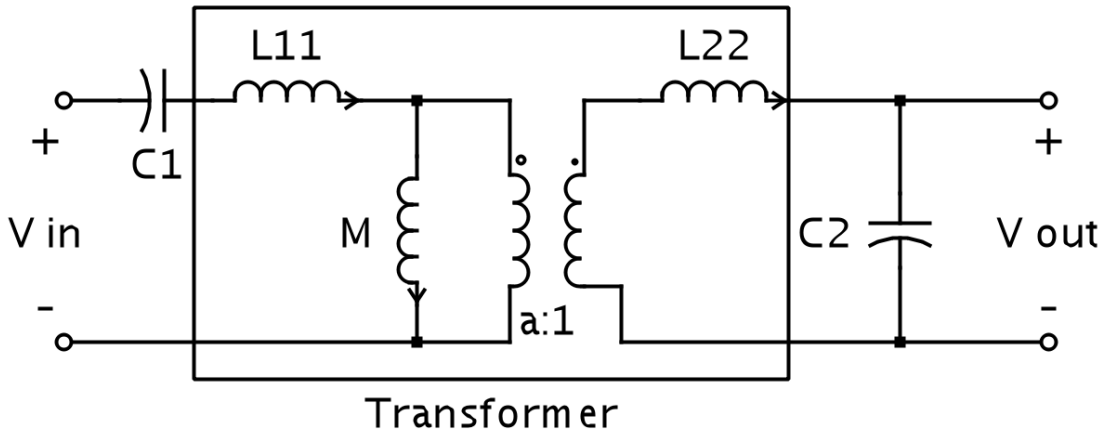


Figure 2.3: Equivalent system model with transformer core.

Table 2: Equivalent circuit component values after considering coupling coefficient

Description	Name	Value
Magnetizing Inductance	M	$k * \sqrt{L_1 * L_2}$
Transmitter Inductance	L_{11}	$(1-k) * L_1$
Receiver Inductance	L_{22}	$(1-k) * L_2$

As evident from the equivalent model and modified component values of the transformer, the coupling coefficient plays a large role in the amount of power that can be transferred. In a vehicle application, the vertical distance between the transmitting coil and the receiving coil found onboard the vehicle can be determined by the ride height of the vehicle, while skew and lateral displacement can be attributed to the human error that comes with the driving a vehicle. A viable range of coupling coefficients has been experimentally determined to be between 0 (when no vehicle is present) and 0.4 (at maximum coupling), though the specific range of operational coupling coefficients will be determined by the system manufacturer [9].

At these low values of coupling coefficient, it is possible to convert much of the energy put into the system to stray magnetic field due to the decreased impedance of the magnetizing inductance. However, the coupling coefficient has a great deal to do with the resonant point of the system. This means that changes in the coupling coefficient can affect the balance of real and reactive power. Loading also affects the ability of the system to transfer power effectively, though the exact effects will be discussed in greater detail later.

2.2 Coupling Coefficient's Effect on System Performance

The model shown in Figure 2.1, the basic wireless series-parallel configuration with a resistive load, has been constructed in MATLAB to reveal the how different coupling coefficients affect the power that can be delivered to a resistive load. In order to analyze the system, a transfer function must be developed that accurately describes the

equivalent circuit diagram. The transfer functions obtained from circuit analysis can be seen below.

$$Z_{eq} = \left[\left(\frac{1}{sC_1} + R_{C1}\right) + (sL_2 + R_{L1})\right] + \left[sk^2\sqrt{L_1L_2} \,||\, \left([s(1-k)L_2 + R_{L2}] + \left[R_L || \left(\frac{1}{sC_2} + R_{C2}\right)\right]\right)\right]$$

$$\frac{V_{in}}{Z_{eq}} = I_{in} \quad , \quad P_{in} = Real\,[V_{in} * (I_{in}^*)] \quad , \quad Q_{in} = Imaginary\,[V_{in} * (I_{in}^*)]$$

For simulations, this system is modeled with a variable resistive load and is powered by a 35 V sinusoidal source of variable frequency. The component values and parasitic resistances for analysis are taken from an experimental system at ORNL and can be seen in Table 3. This system is tuned to be resonant at 22.6 kHz. Simulating the system with these values over a variety of operational frequencies and coupling coefficients reveals the real power, reactive power, and system efficiency plots found in Figure 2.4-Figure 2.6, respectively. The same two points have been marked on each graph. The first is the point at which the maximum power is transferred to the load. This point shows a power transfer of 7.6 kW and is at a coupling coefficient of 0.055 and a frequency of 22.6 kHz. However, this point is only 52% efficient. The second point shows a power transfer of 2.7 kW. This data point is at a coupling coefficient of 0.15 and a frequency of 22.6 kHz and shows a dramatically increased efficiency of 87%.

Table 3: Component values of the simulated WPT system

Transmitter		Receiver	
L_1	36.6 μH	L_2	36.6 μH
R_{L1}	38 mΩ	R_{L2}	38 mΩ
C_1	1.36 μF	C_2	1.36 μF
R_{C1}	1 mΩ	R_{C2}	1 mΩ

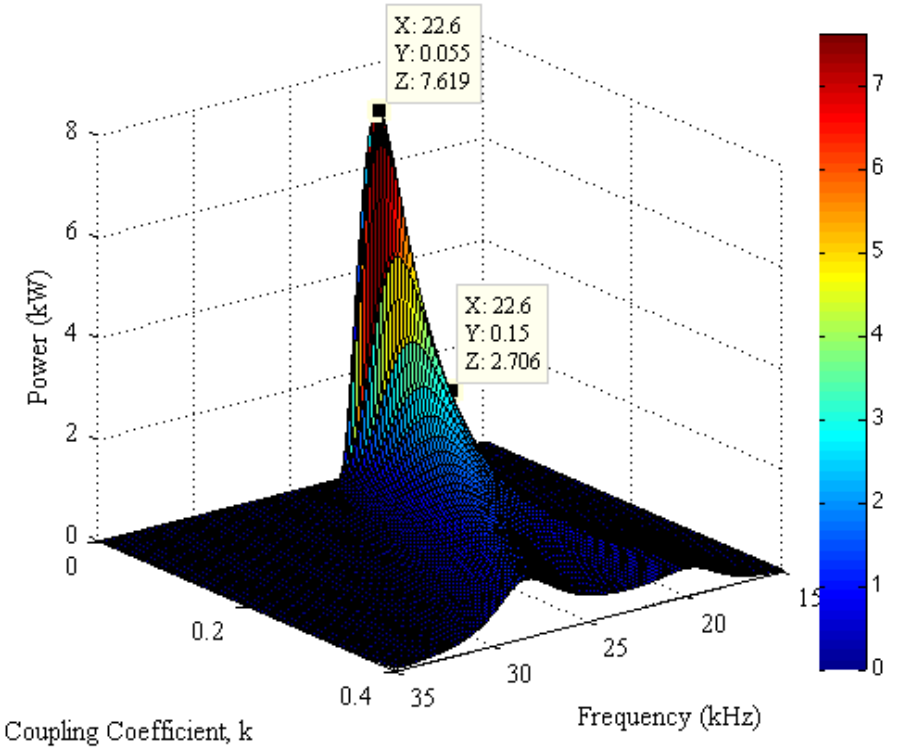


Figure 2.4: Output power versus coupling coefficient and frequency.

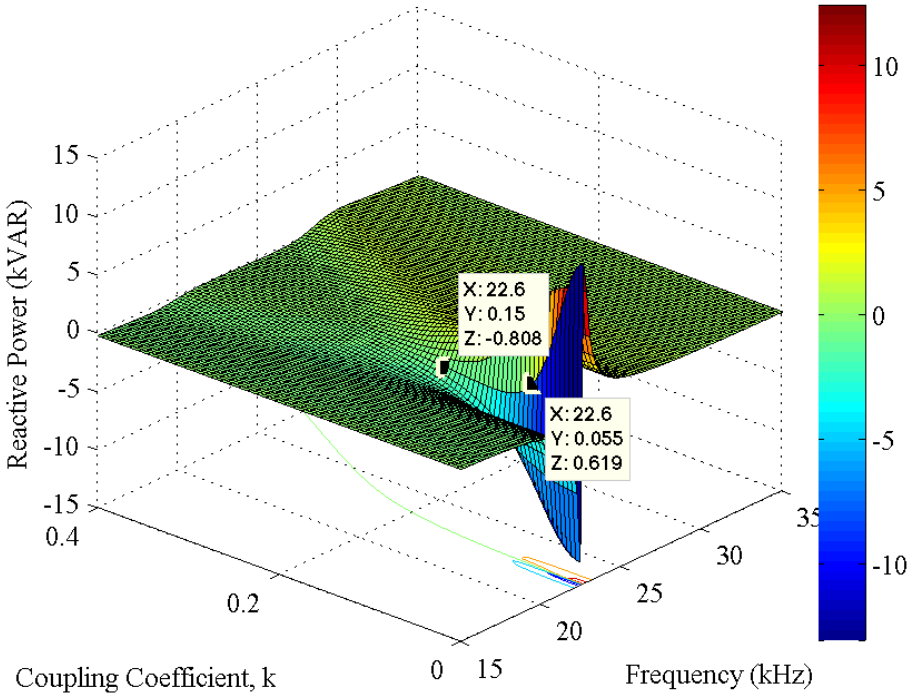


Figure 2.5: Input reactive power versus coupling coefficient and frequency.

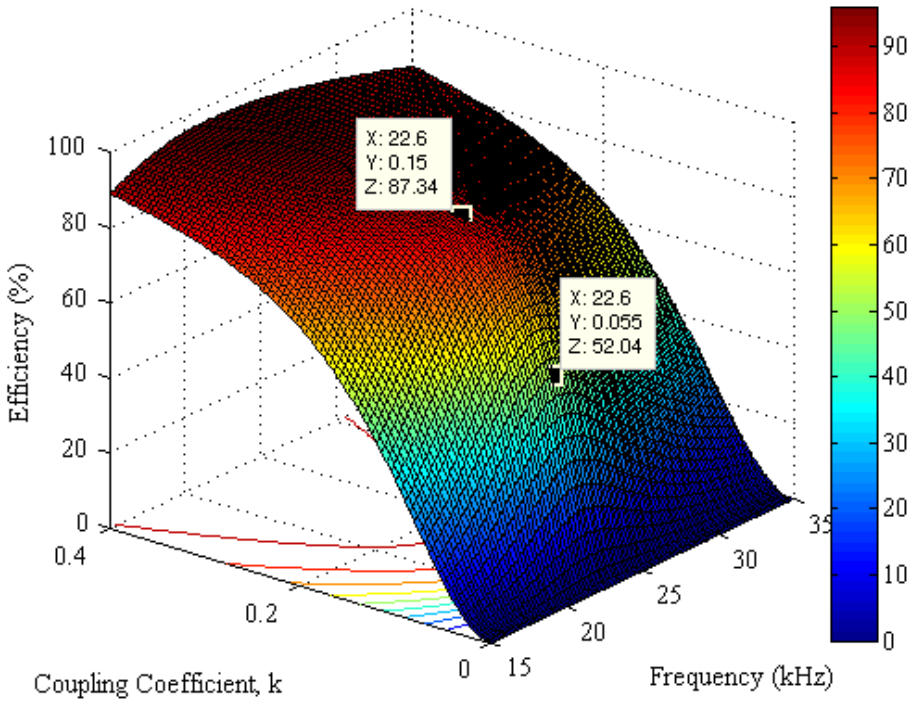


Figure 2.6: System efficiency versus coupling coefficient and frequency.

In order to obtain a better view of the effects, Figure 2.7-Figure 2.9 show the input real and reactive power (P_{in} and Q_{in}) and the output power (P_{out}) for coupling coefficients of 0.15, 0.3, and 0.4 versus frequency, respectively. As the coupling coefficient increases, the system reaches a point at which bifurcation appears in the input real and reactive power and the output power. This shows that the coupling coefficient has a significant effect on the resonance point of the system. As the coupling coefficient increases, the leakage inductance of the air gap transformer changes values, resulting in a difference in resonant points between the transmitter and receiver and leading to the noted bifurcation. Coupling coefficients over 0.707 result in a bifurcation large enough to result in multiple zero crossings in the reactive power curve. The reasoning for this will be discussed later in the section.

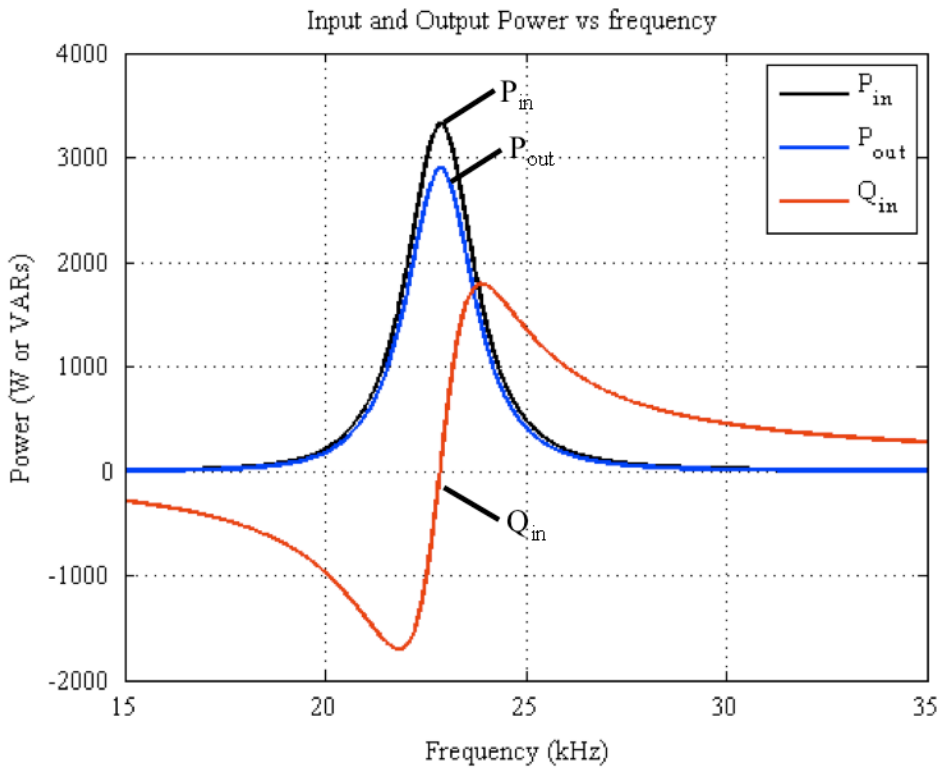


Figure 2.7: P_{in}, P_{out}, and Q_{in} versus frequency for a coupling coefficient of 0.15.

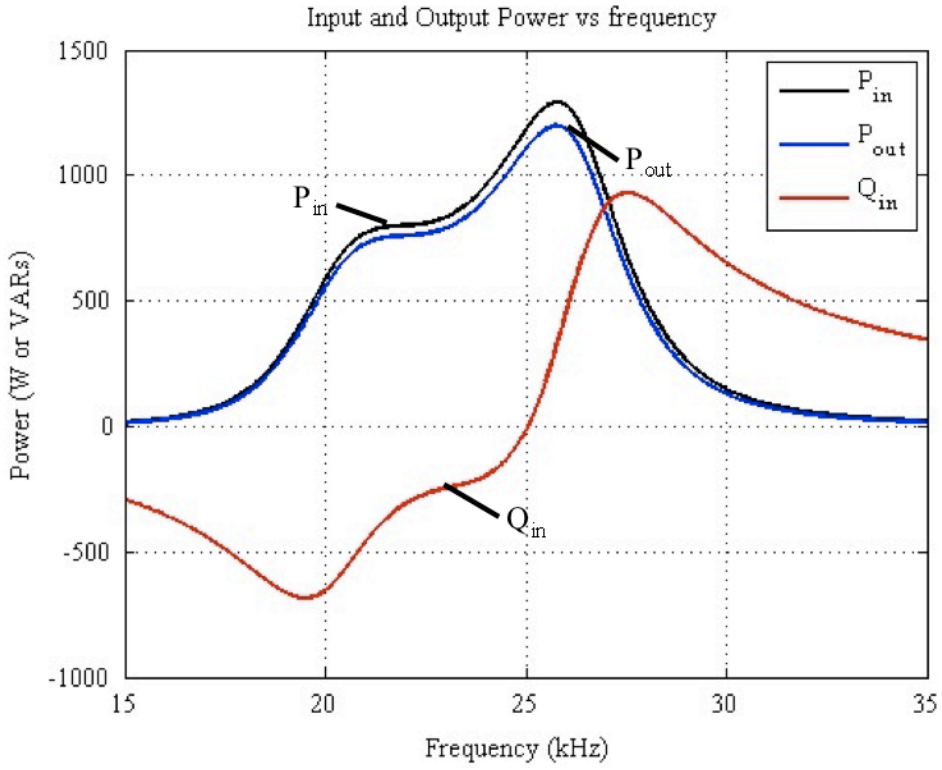


Figure 2.8: P_{in}, P_{out}, and Q_{in} versus frequency for a coupling coefficient of 0.3.

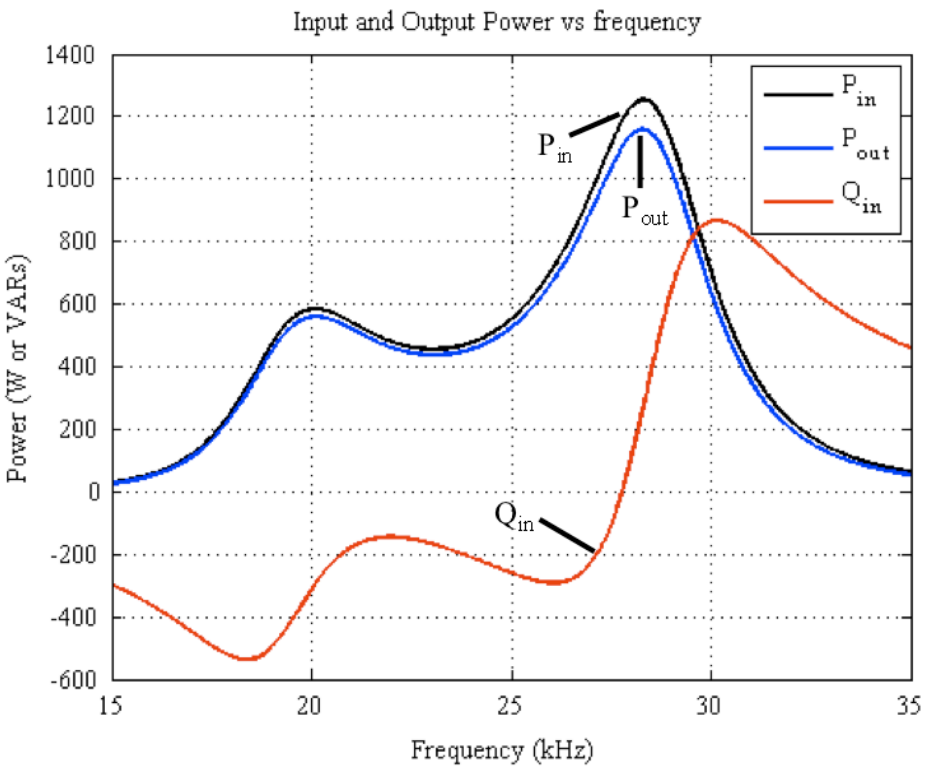


Figure 2.9: P_{in}, P_{out}, and Q_{in} versus frequency for a coupling coefficient of 0.4.

2.3 Resistive Load's Effect on System Performance

Load characteristics also have a significant role in the amount of power that can be transferred by a system. From Figure 2.10 we can see that if the value of the load's resistance is too high, the system can have a large bifurcation similar to those shown in the previous section. This can also result in multiple zero reactive power crossing frequencies, as shown in Figure 2.11. On the other hand, Figure 2.12 can be used to show that if the load has too low a resistance, the system can have much of its real power dissipated in the parasitic resistances of the transmitting and receiving circuits, resulting in a low maximum efficiency.

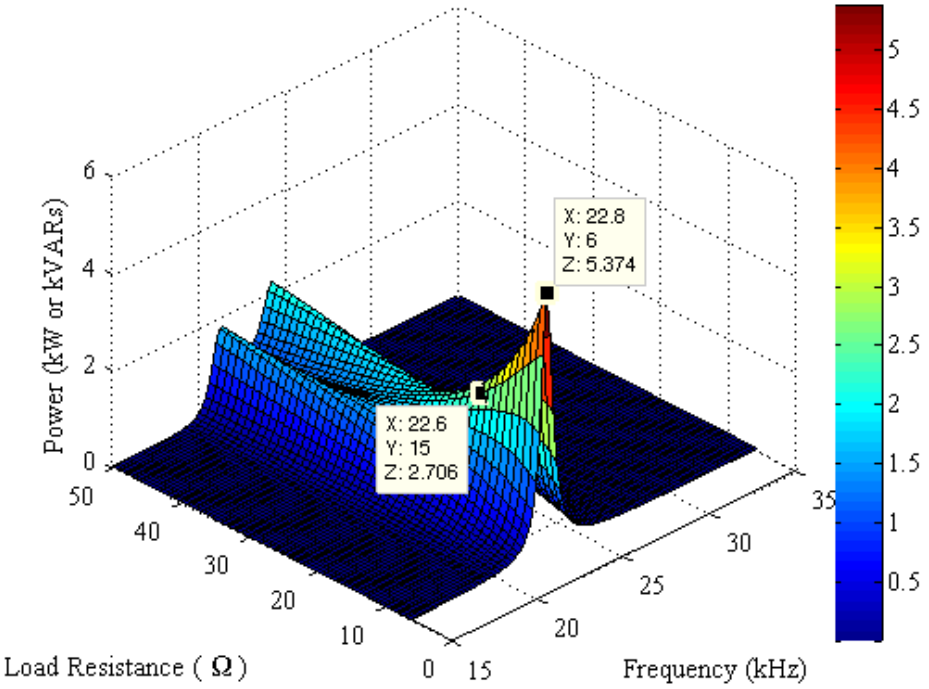


Figure 2.10: Output power versus load resistance and frequency.

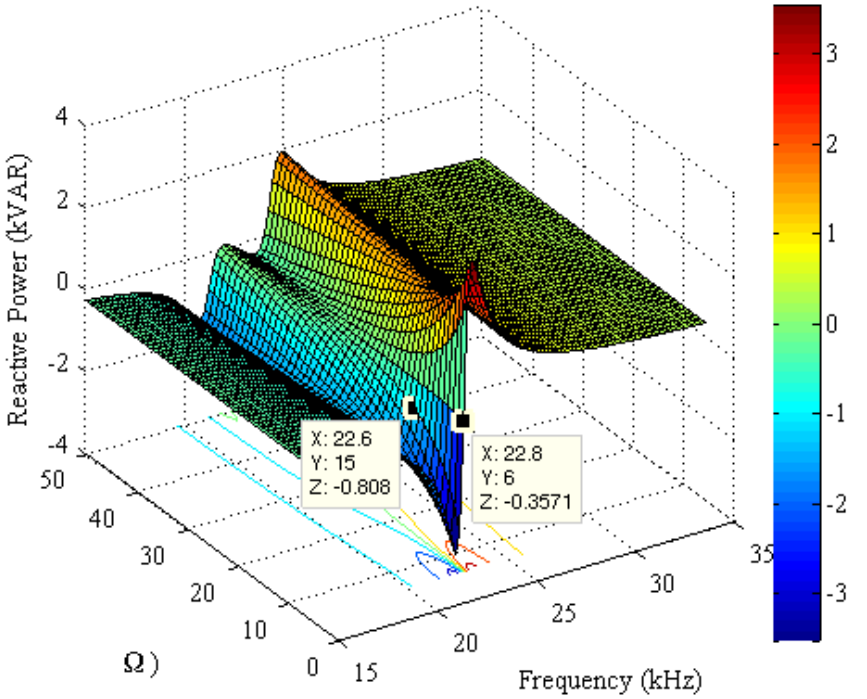


Figure 2.11: Input reactive power versus load resistance and frequency.

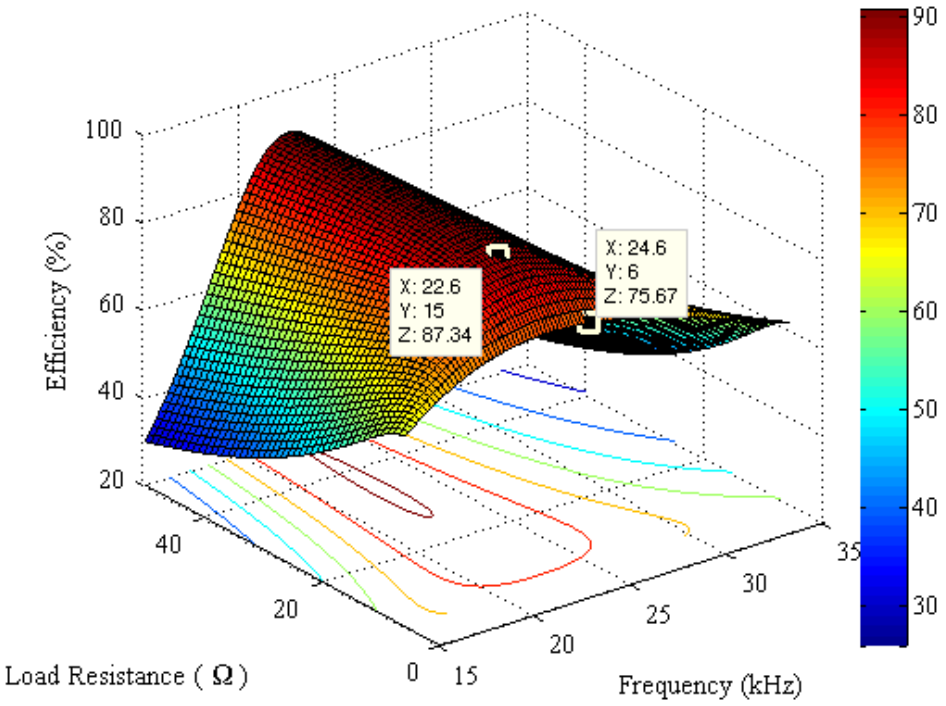


Figure 2.12: Efficiency versus load resistance and frequency.

As stated before, a high load resistance introduces the possibility of two relative maximum power points for a stated load resistance and coupling coefficient. While this is not a problem itself, the window of frequencies that show high system efficiency narrows as the load resistance increases. The peak efficiencies frequencies occur slightly higher than the lower frequency local maximum.

To get a better view of the effects of the load resistance on the transfer system, load resistances have been selected and analyzed at a coupling coefficient of 0.15. The loads are 15 Ω, 30 Ω, and 40 Ω in Figure 2.13-Figure 2.15, respectively. As the load resistance increases, the bifurcation in power transferring capability in the real power plots grows. When the load resistance becomes large enough, a bifurcation also appears in the reactive power plot.

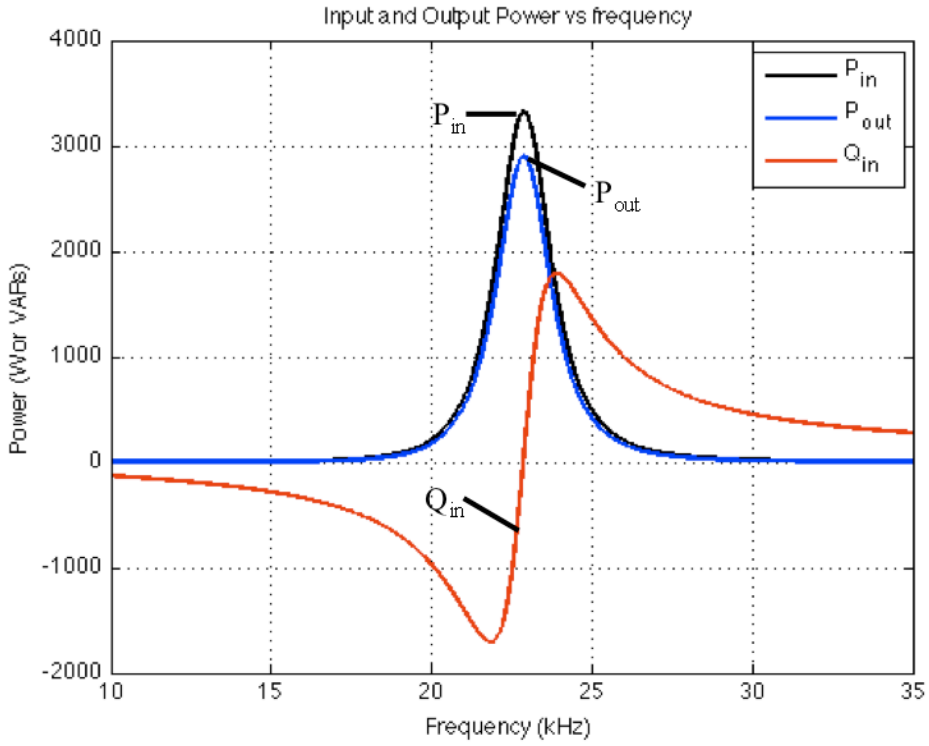


Figure 2.13: P_{in}, P_{out}, and Q_{in} versus frequency for a load resistance of 15 Ω.

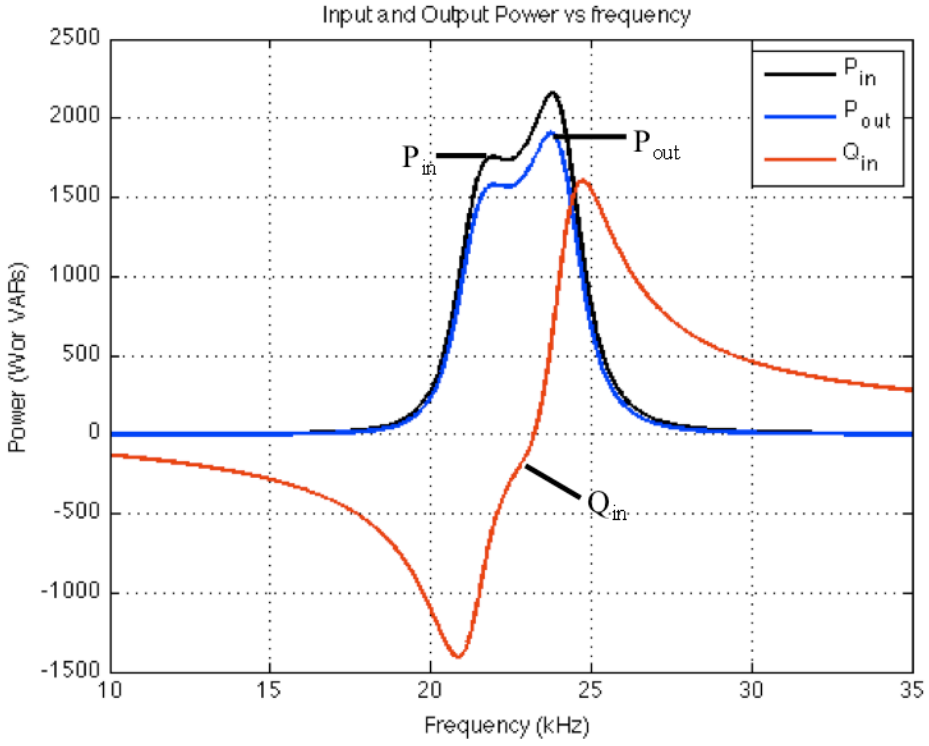


Figure 2.14: P_{in}, P_{out}, and Q_{in} versus frequency for a load resistance of 30 Ω.

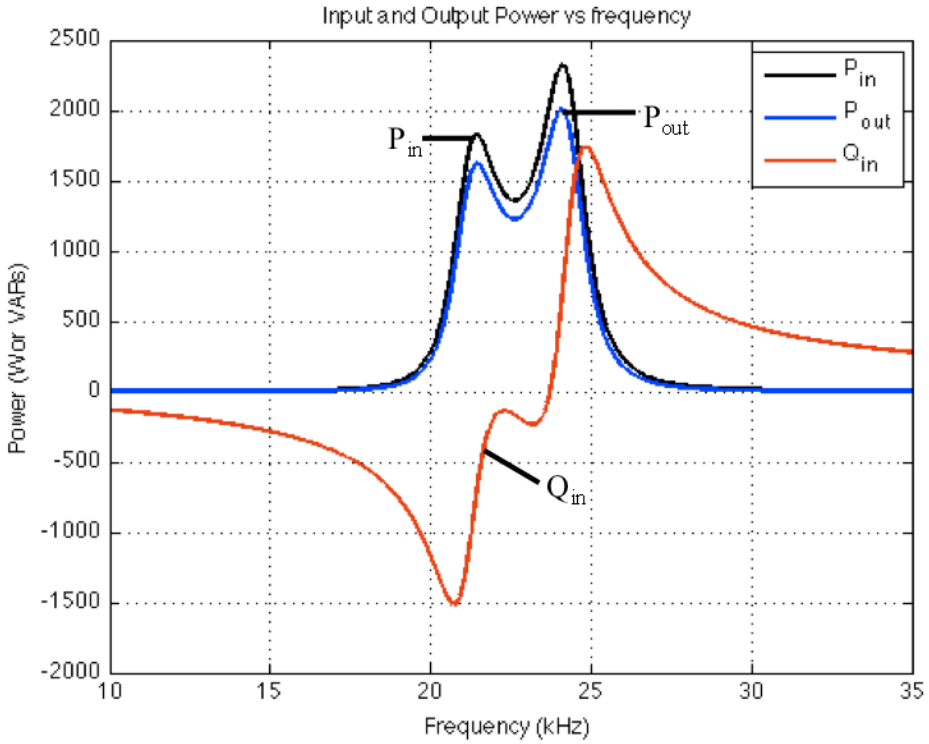


Figure 2.15: P_{in}, P_{out}, and Q_{in} versus frequency for a load resistance of 40 Ω.

The bifurcation of the reactive power trace occurs when the load resistance reaches a critical level. This level is determined by the coupling coefficient and the component values within the system. The equation for this critical impedance is shown below [10]. Example values of the critical impedance for various coupling coefficients for the example system can be shown in Table 4.

$$Z_C = \sqrt{\frac{L_2}{C_2}} \quad , \quad Z_{CRIT} = Z_C * \sqrt{\frac{1-k^2}{k^2}}$$

Table 4: Critical impedances for various coupling coefficients

Z_C	k	Z_{CRIT}
5.2 Ω	0.15	34.2 Ω
-	0.30	16.5 Ω
-	0.40	11.9 Ω
-	0.707	5.2 Ω

In Figure 2.15, the load resistance is greater than Z_{CRIT} and shows a bifurcation in the reactive power plot. When the load resistance increases beyond 47.5 Ω for the coupling coefficient of 0.15, the reactive power plot for this system contains multiple zero crossing frequencies. When k is approximately 0.707 Z_C equals Z_{CRIT}. This means that the reactive power is guaranteed to possess multiple zero reactive power frequencies.

2.4 Problem Statement Summary

WPT is based on magnetic coupling between a transmitting and receiving coil in found in resonant circuits. If the transmitter and receiver are tuned to the same resonant frequency, power can be transferred between the circuits via a magnetic field. The exact amount of power that can be transferred for an input voltage level depends on the coupling coefficient and the characteristics of the load. Though much work remains before large-scale adoption can begin, electric vehicles can greatly benefit from WPT if it is employed correctly.

Chapter 3 Literature Review

3.1 Introduction

Wireless power transfer is currently a popular topic of study. Much of the research performed for WPT has been targeted at improving the range and resistivity to skew of the transfer systems to improve overall system performance. While these are very important issues that need to be looked into, the issue of the potential for poor power is also important. This section will highlight research being performed in both areas.

3.2 Research to Increase WPT Coupling

The most common research topics within WPT are increasing the space at which the coils can be separated and reducing the impact of misalignment on the transfer circuits. One of the most prevalent ways to increase the amount of power transferred from the transmitter to the receiver is to add a magnetic backing material. A second possible solution to increase range is to use additional coils to shape the magnetic field. The most common range extending technique is to use a track system for in-motion charging.

By adding a backing material, such as aluminum plating, stray magnetic fields can be reduced or shaped in such a way that they can be more easily coupled to receiving coils [11]. A backing plate that is larger than the receiving coil further increases the effect by allowing more flux to become coupled and reducing the stray fields [12],[13]. By using these materials to absorb stray inductance, it helps to shape the field in an upward direction allowing more magnetic flux to pass through the receiving inductor. Significant improvements in coupling coefficients have been reported when using backing materials, resulting in higher power transfer capabilities.

Another way to shape the magnetic field so that more flux passes through the receiver is to use multiple transmitting or receiving coils [14], [15]. One example transmitting coil design uses a DDQ-DD design to reduce the effects of skew on the coupling coefficient [16]. This design uses multiple coils on both the transmitter and receiver and can be seen in Figure 3.1. When multiple separate coils are used in an array, the likelihood that there is a high coupling coefficient can be obtained is increased, reducing the effect of skew on the system.

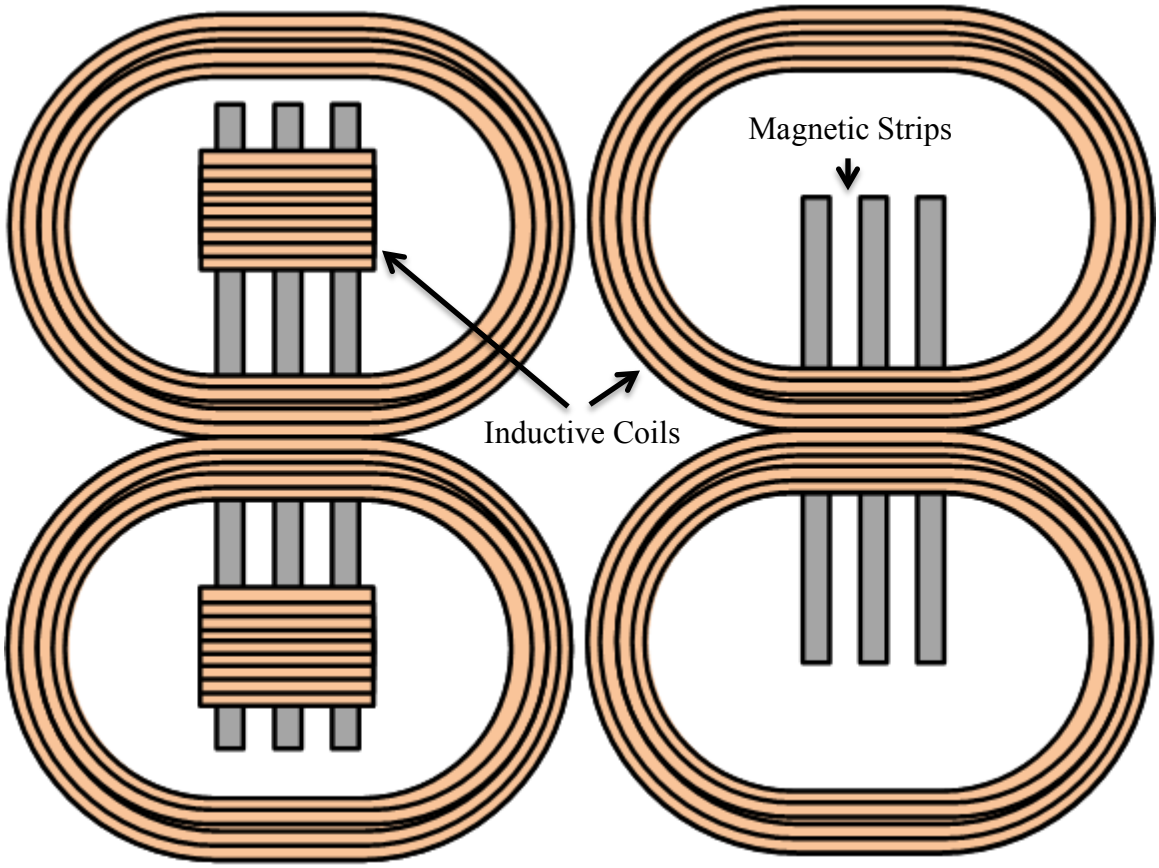


Figure 3.1: DDQ-DD coil configuration

However, using multiple coils complicates the overall system, increasing cost and potentially increasing losses due to stray fields and increased resistance. Though adding coils to the receiving system may help to improve the coupling coefficients between the transmitter and receiver, the addition of components leads to an increase in system cost and weight. To combat the losses of stray fields, a control signal can be used to determine which coils should be active, though this will also increase system prices. When coils are used in an array, the proximity effect plays a greater role because of the increased magnetic field strength from the additional coils. This increase in resistance may lead to an uneven distribution of transfer and further reduce the overall system efficiency.

Another way to increase the range of a single transmitting coil is to extend the transmitting coil into a track shape [17],[18]. In making a track system, a single coil and inverter used to provide power to one or more receivers over a pre-specified length. It creates a simple way to provide power over a significant range and increases the length of time that the coupling coefficient remains constant by reducing the effects of driving over the end of the coils. When passing over the end of the track system, there is an increased likelihood in which the magnetic field passed into and back out of the middle of the receiving coil, resulting in no field intersection. This type of transmitter could also potentially charge multiple receivers at once.

Unfortunately, this type of transmitter creates unnecessarily large amounts of stray magnetic field if the track is not completely coupled to the maximum number of receivers. The stray magnetic fields can also be a hazard to nearby pedestrians since there is no shielding, though magnetic shielding for public transportation has been examined. Another issue with a track system is that multiple coupling coefficients must be

considered when performing reactive power compensation techniques through the inverter. In this system, it is likely that reactive power compensation would need to be performed at the receiver, increasing the cost to automotive manufacturers.

3.3 Power Factor Correction

There are two main ways of correcting for power factor at the inverter. The first of which is to use an inverter that tracks the zero crossing frequencies for operating systems. The second is to use additional circuit components in the transfer system itself to force the system to operate at unity power factor.

A significant amount of research has been performed in tracking the frequency of the zero reactive power points for a system [19]-[21]. Using this type of power factor correction will not require additional components the transmission system. However, when using this type of control, there may be difficulties responding fast enough to eliminate the reactive power from the system for in-motion chargers. Another issue is that it will require precise measurements to accurately determine the angle between the voltage and current waveforms.

When used in high power applications, the inverter is less likely to perform advanced switching methods because of the speed limitations on high power transistors. This means that the inverter is likely to perform quasi-square wave operation, making the system highly dependent on timers when performing real and reactive power computations.

One of the popular methods that have been used to correct for the low power factor has been to add second inductor in series with the load terminals on the receiving circuit [22]. While this has had promising results, adding components to the vehicle is not

in the best interest of the system. By increasing the components the vehicle, the power required to move the vehicle is increased and auto manufacturers are less likely to adopt the technology due to increased cost.

3.4 Literature Review Summary

Researchers are currently trying to improve WPT so that it may be more widely adopted by manufacturers and the public. Ways of improving the coupling coefficient between the transmitter and receiver are being explored in a number of ways. These include using backing materials to reduce stray fields, using transmitting and receiving arrays to improve the chances of high coupling, and the use of inductive tracks to allow moving vehicles to charge for a greater amount of time. Other research is being performed to reduce the reactive power demands from the transmission system. There is much work to be done before the technology is ready for widespread adoption, but researchers are actively pursuing solutions to these problems.

Chapter 4 Wireless Power Transfer Simulations

4.1 Simulation Development

Since the target of this paper is to address the grid's view of the WPT system, a model must be developed that accurately describes the loading conditions that may describe a real WPT system. The block diagram found in Figure 4.1 describes one possible system, though two specific systems will be evaluated. This will require a range of subsystems to be developed. PLECS will be used for the simulations. Four of these subsystems stand out against the rest for their relative complexity. The transfer system will be analyzed first to show the validity of the model. It will be based on the same system as in previous chapters. In order to help regulate the power level coming through the transfer system, a simple quasi-square wave inverter and a non-inverting buck-boost converter will be modeled. Then, the different kinds of power factor correcting rectifiers will be discussed, and one will be selected for simulation.

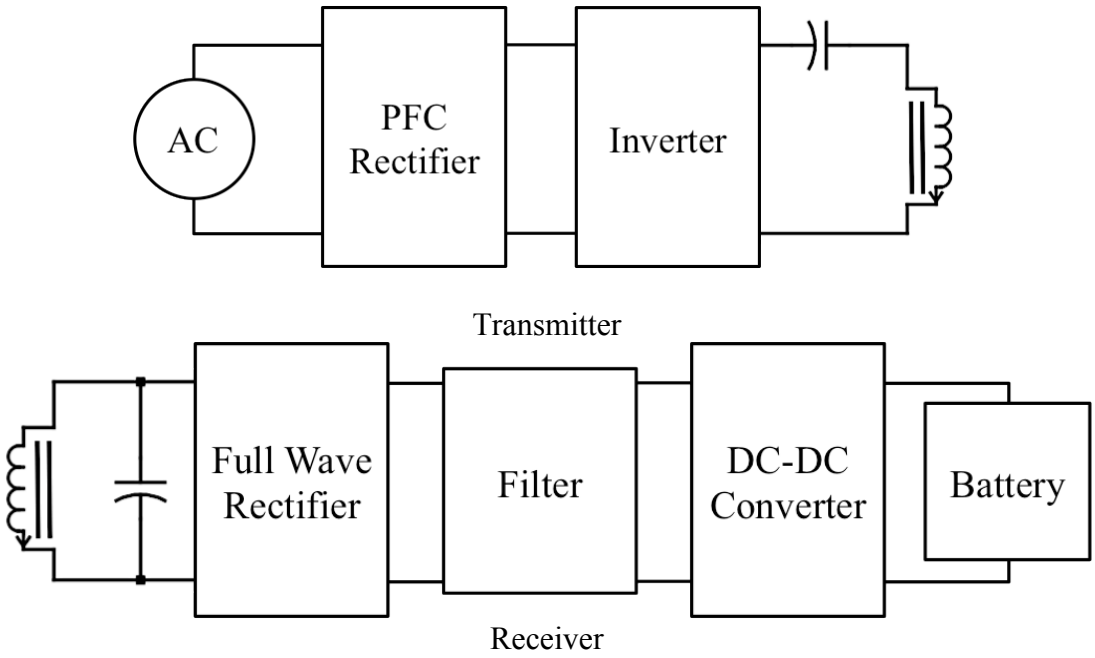


Figure 4.1: Receiver controlled system block diagram.

4.1.1.1 Transfer System

The most important part of the model is the WPT system. This consists of a series tuned transmitter and a parallel tuned receiver, as in previous chapters. To verify the model, the values from ORNL's system are implemented and compared with experimental results. Figure 4.2 and Figure 4.3 show the simulated model and the coils from the system they model.

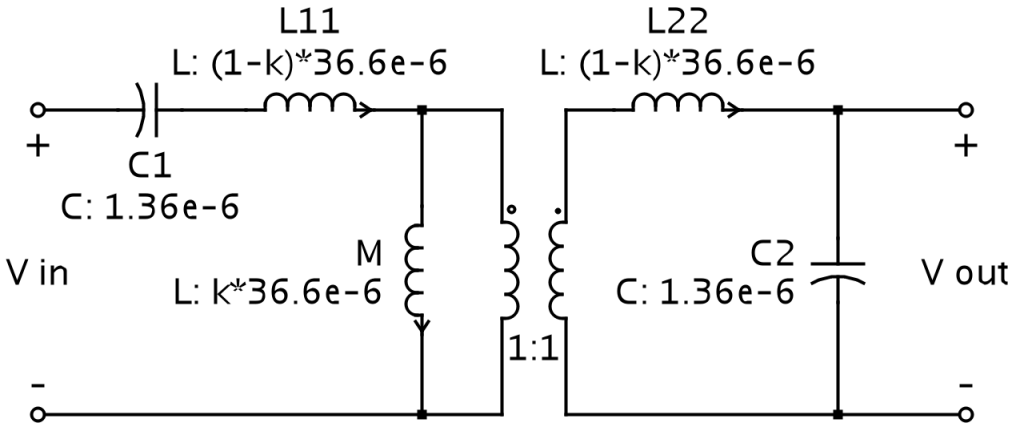


Figure 4.2: Series-parallel WPT simulated system.

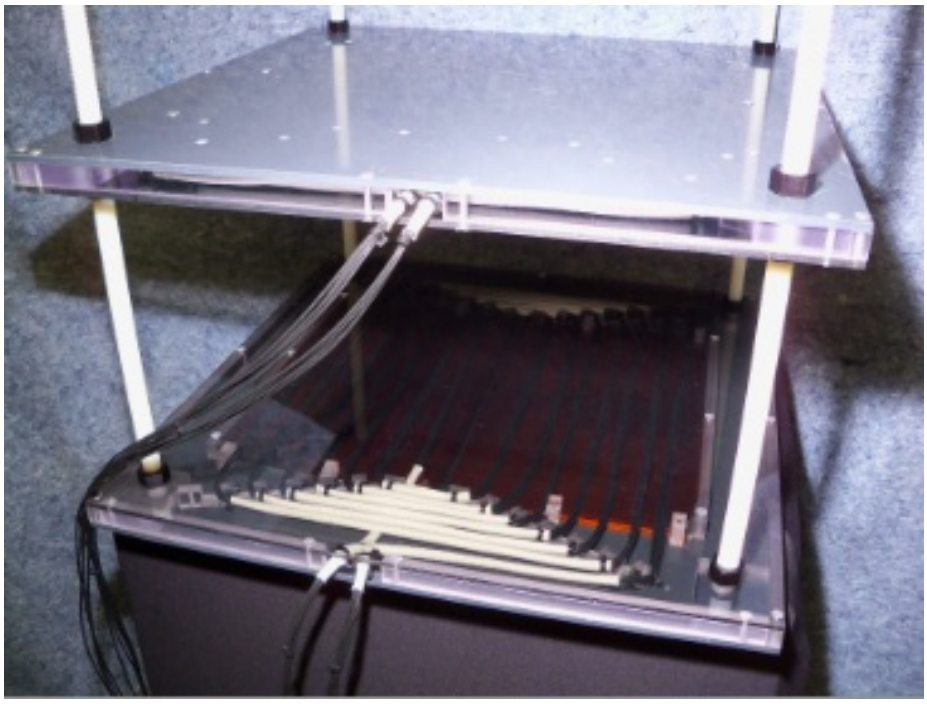


Figure 4.3: Coils from the system which the simulated system is modeled.

The system from which the simulation model is taken consists of a set of coils, their tuning capacitors, a battery eliminator load, and a high frequency inverter. The battery eliminator load is a light bank that maintains a constant voltage. When a light is fully powered, the excess power from the system is delivered to the next light in the bank. This continues until all available power is used. This allows for a visual representation of the power being transferred across the coils.

Before the rest of the system can be analyzed, the WPT system needs to be inspected to ensure that they operate in a similar fashion to the actual system. The system described above was used to obtain experimental data with which to compare the model. The waveforms in Figure 4.4 were obtained by operating the experimental system at a coupling coefficient of 0.2 and an operational frequency of 20 kHz. The top two plots reveal the input voltage and current to the transfer system. The voltage waveform shows quasi-square wave operation of the high frequency inverter. Output voltage and current waveforms can be seen in the bottom two plots.

The simulated system was tested under similar conditions as the experimental system, though without a model for the load bank, some differences can be expected. A controllable voltage source that operates in the same fashion as the experimental system was used in place of the inverter. As expected, small differences can be noted in the output of the experimental system shown in and the simulated system in Figure 4.5. This is because of the high dependency on load characteristics and coupling coefficients and the model's use of ideal components in the load bank. The model has proven to be accurate enough for further simulation.

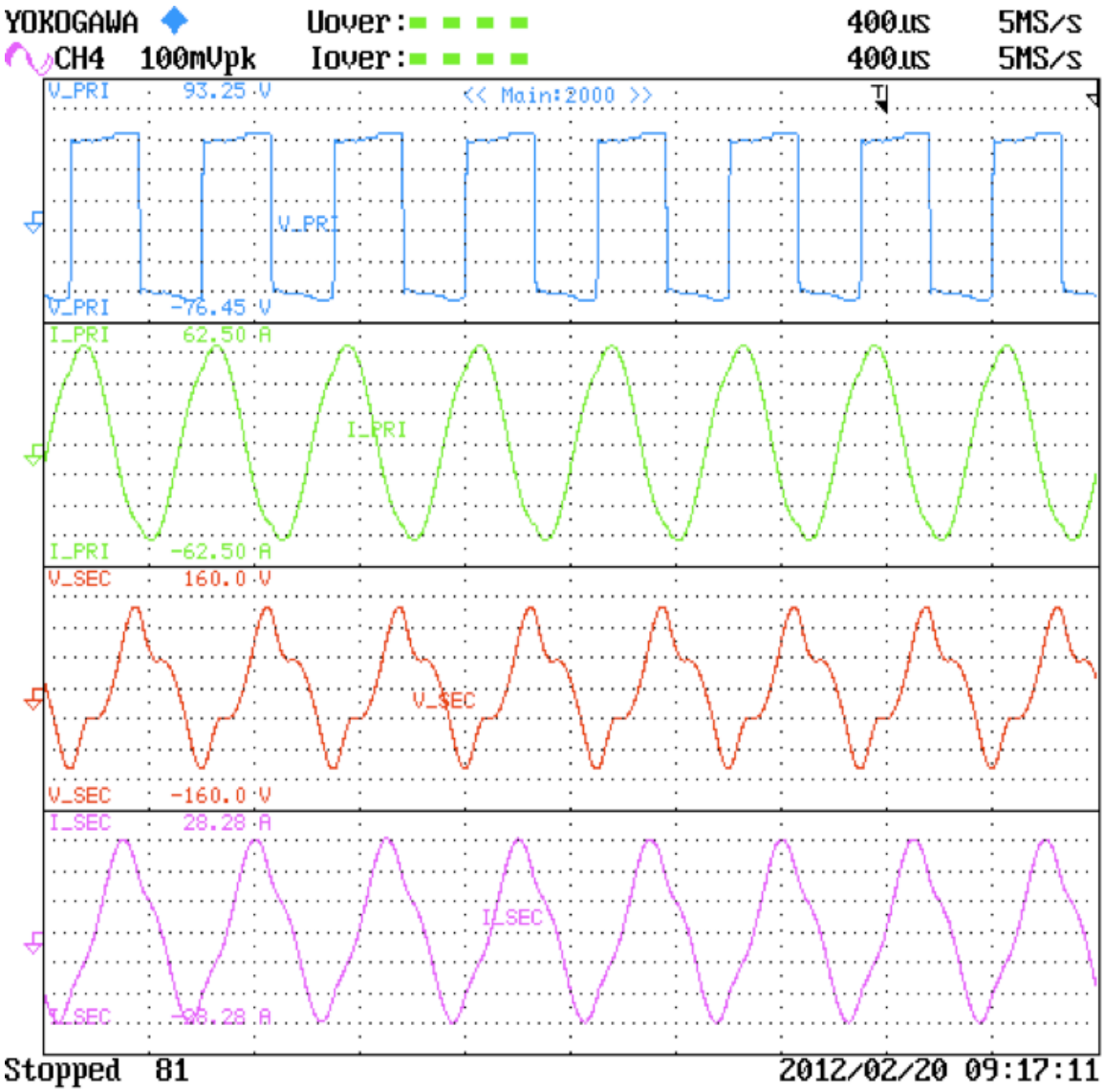


Figure 4.4: Experimental results for WPT system at ORNL.

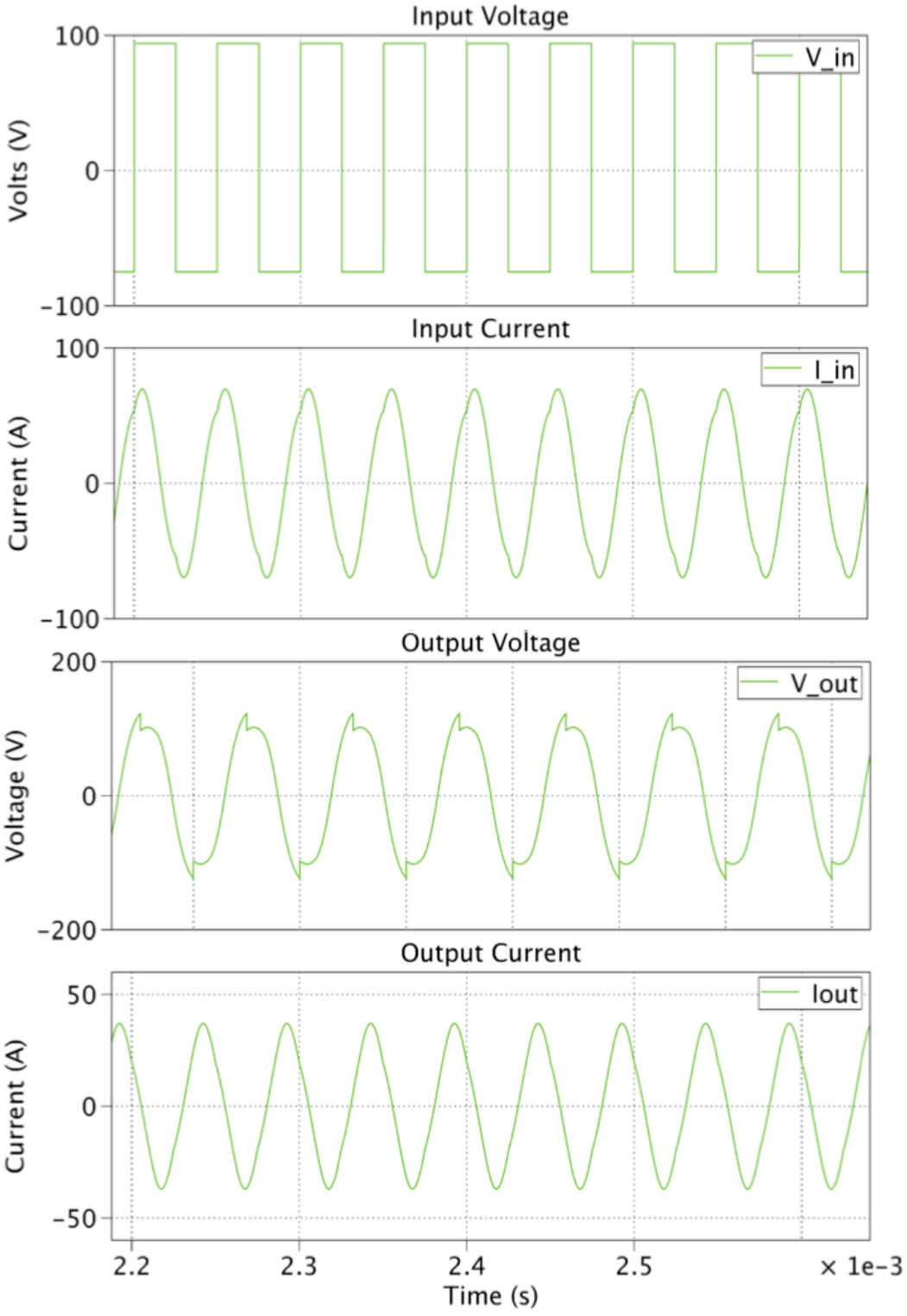


Figure 4.5: Simulated results of WPT system at ORNL.

When tested with the transfer system and a rectifier, it should be noted that the reactive power of any filtering components will draw reactive power. This holds true when the resistive load is exchanged for a voltage source, such as a battery. Another important change when a resistive load is exchanged for a voltage source is that the source will absorb reactive power from the system because it can absorb current that is out of phase with the voltage. This measurement was taken at the input to the rectifier on the receiver system. The tabulated results from two of these tests (performed at 22.9 kHz and a coupling coefficient of 0.15) can be seen in Table 5.

Table 5: Results from quasi-square input voltage testing

	Resistor Load Test	Voltage Source Test
P_{in}	1987 W	1980 W
Q_{in}	-24 VAR	-715 VAR
P_{out}	1787 W	1760 W
Q_{out}	0 VAR	-697 VAR
Efficiency	90 %	89 %
Input Power Factor	1	0.94

4.1.1.2 Inverter

The inverter is the second key component in the simulation. It controls the operating frequency and determines how much power will be transferred to the transfer system. To accurately depict the operation of a high power inverter at operational frequencies, the system will operate in a quasi-square wave fashion. The output frequency of the inverter and duty cycles of the output waveform will be manually controlled.

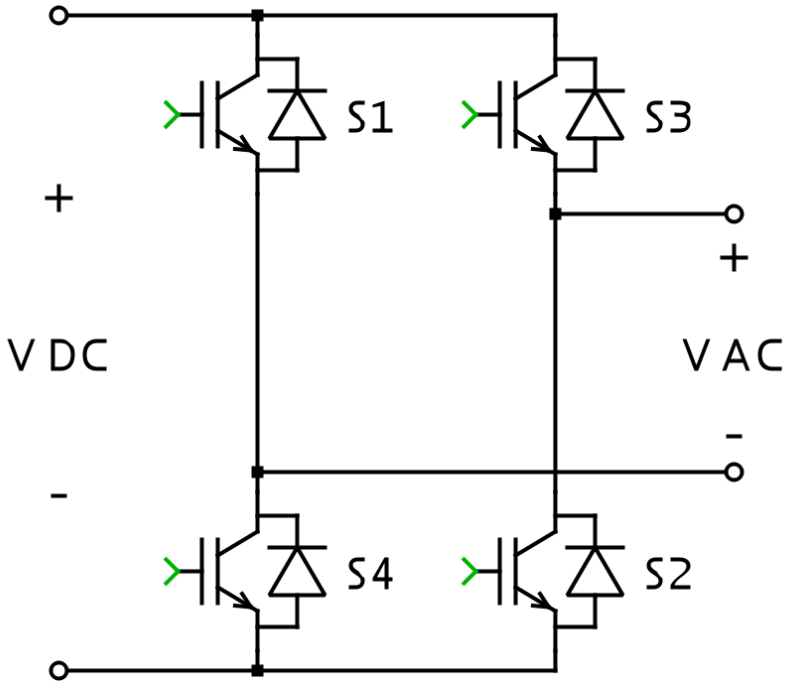


Figure 4.6: Inverter model.

4.1.1.3 Non-Inverting Buck-Boost Converter

In order to regulate the amount of power going into the vehicle's battery, a buck-boost converter will be employed. This converter will be a non-inverting system and will consist of a buck converter in series with a boost converter, as shown in Figure 4.7, to allow separate control of the two converters. In an effort to provide a better control system, the converter will have three modes of control to compare the control strategies of each. When in boost operation, the buck converter switch is set to always conduct. Conversely, when in buck operation the boost converter switch is turned off.

Because the battery model used has a small internal resistance, the differences in the minimum and maximum output voltages were relatively small. Though the measurement is enough to obtain control of the device in all tested cases, this control loop had the worst current ripple. Because of the limitations on voltage control due to the small internal resistance, the current control loop yielded more promising results. The ripple current and voltage in independent testing proved to be less than 2% of the specified value. With the voltage control having the worst ripple, the feedback loop containing both current and voltage control only operated slightly better than the current only control loop.

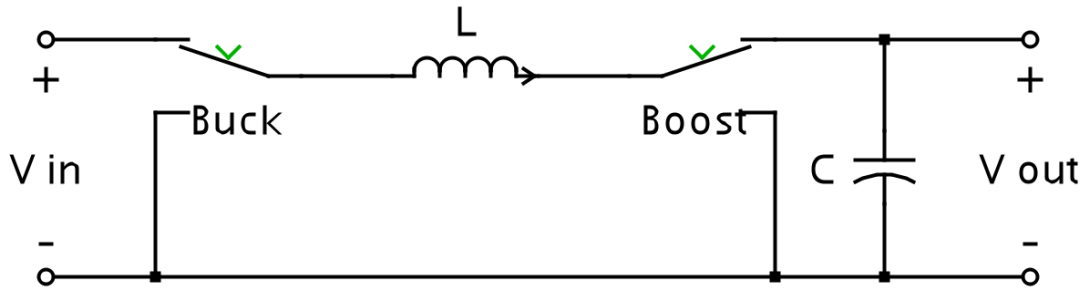


Figure 4.7: Non-inverting buck boost DC-DC converter.

4.1.1.4 Power Factor Correcting Rectifier

In order to achieve the desired power factor across all loading possibilities, a power factor correction (PFC) rectifier was modeled. There are a number of different topologies for a PFC. These include active rectifiers that use transistors to shape the input current and passive rectifiers followed by a DC-DC converter to control the input current [25],[26]. Each model has its advantages and disadvantages, which will be briefly discussed.

Active rectifiers use transistors arranged in an H-bridge configuration to control the input current directly. These can also be used to reduce the DC voltage level by controlling the duty cycle of the switches. While a three phase active rectifier can be easily converted to DQ coordinates for simpler control, a single-phase system is more complex. The model for an active rectifier can be seen in Figure 4.8. The disadvantages of the active rectifier are increased cost when compared to a passive rectifier and the need of an input filter when buck operation is desired.

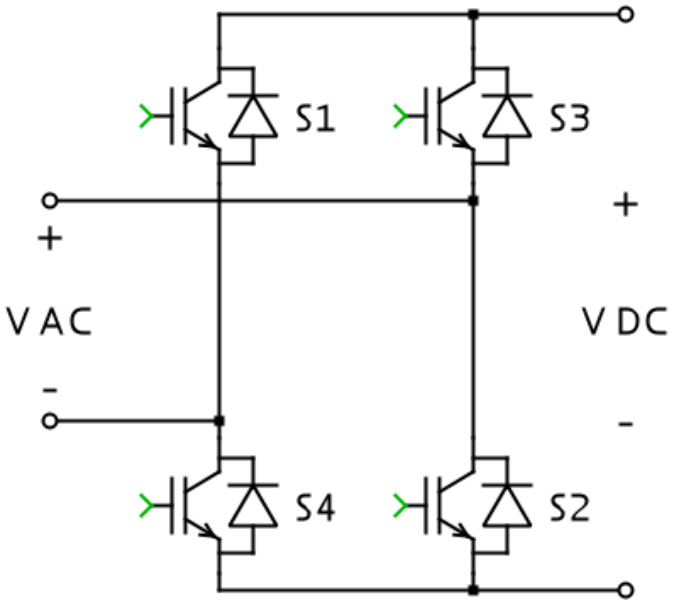


Figure 4.8: Active rectifier.

Another possible power factor correction circuit is a passive rectifier that would be followed by a boost converter. This has the advantage of being able to directly control the input current with a low total harmonic distortion (THD) without the need for an input filter. However, this system can only operate in voltage boosting mode, so voltage reductions will need to be completed by controlling the duty cycle of the high frequency inverter. Another disadvantage is that the system is only viable for a single-phase input.

The control system for the model constructs the reference current and uses the single switch to recreate said current. The reference current is constructed from two voltage measurements. First, the current grid voltage is measured and compared with a peak voltage value. This gives the control loop a unity phase measurement. Second, a voltage measurement is made from the DC link voltage, which is used to make magnitude adjustments. This model can be seen in Figure 4.9.

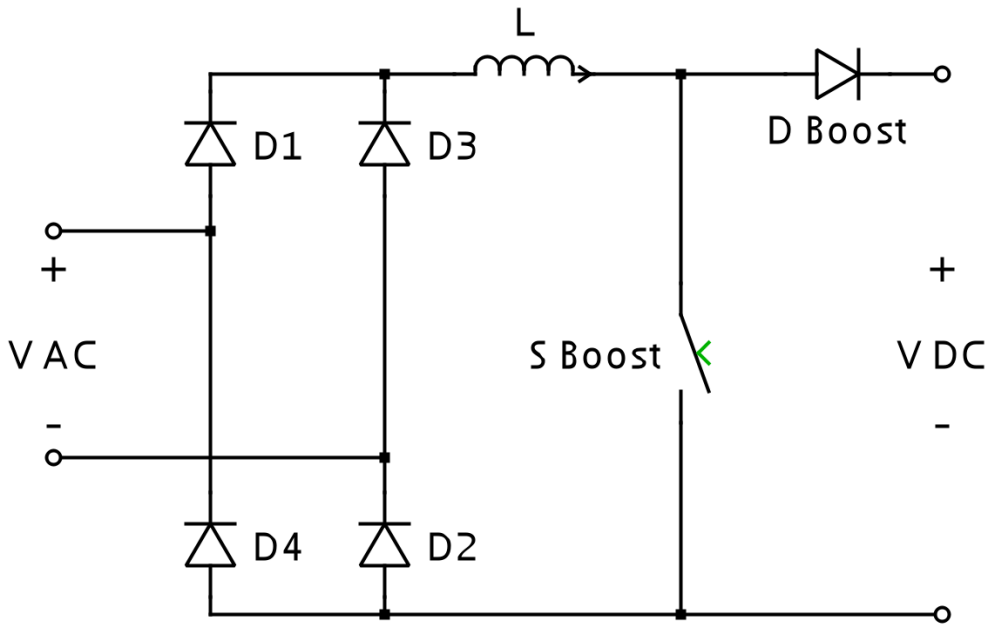


Figure 4.9: Selected PFC rectifier.

4.2 Receiver Controlled System Simulation

With the subsystems for the model designed and tested, an ideal voltage source was placed in the circuit that would represent the utility. The overall system found in Figure 4.1 will be simulated at various coupling coefficients to represent different vehicle ride heights and misalignments. The system will be requested to send 2 kW and 4 kW to a designated vehicle battery voltage. The buck-boost converter on the receiving circuit will perform voltage regulation for the initial round of simulations. This model was used for the International Electric Vehicle Conference in March of 2012 [27].

The first simulation to be examined with this model was run at 20 kHz at a requested power load of 2 kW and a coupling coefficient of 0.15. Without power factor correction, the utility voltage and current can be seen in Figure 4.10. Figure 4.11 reveals that the power factor correction device was able to bring the displacement power factor to unity and has a THD of 3.9 %. The battery charging voltage and current can be seen in Figure 4.12.

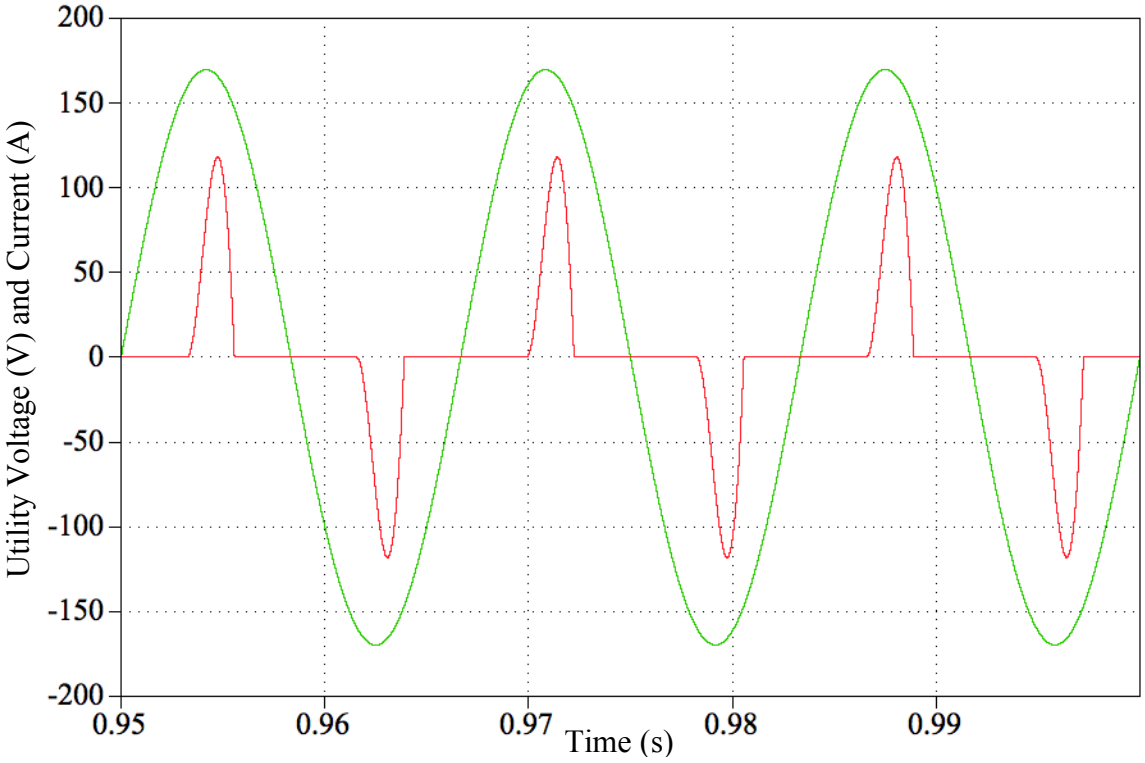


Figure 4.10: Receiver controlled system without PFC (2kW test).

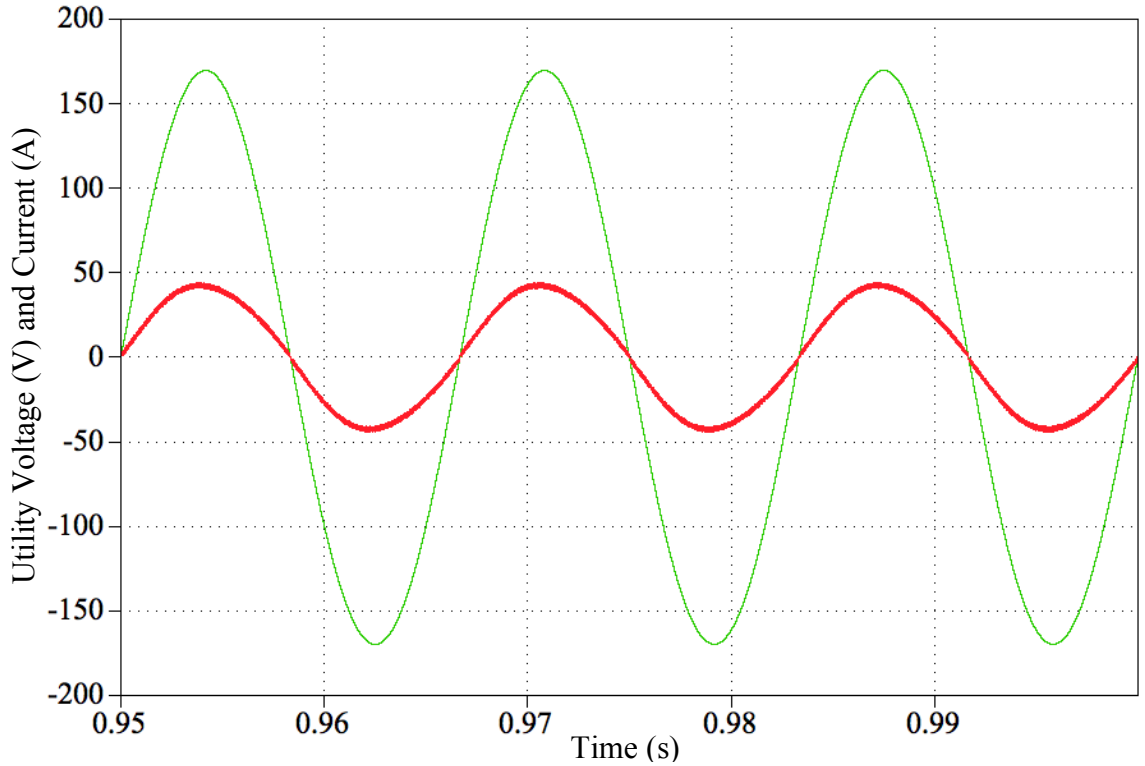


Figure 4.11: Receiver controlled model utility voltage and currents (2 kW test).

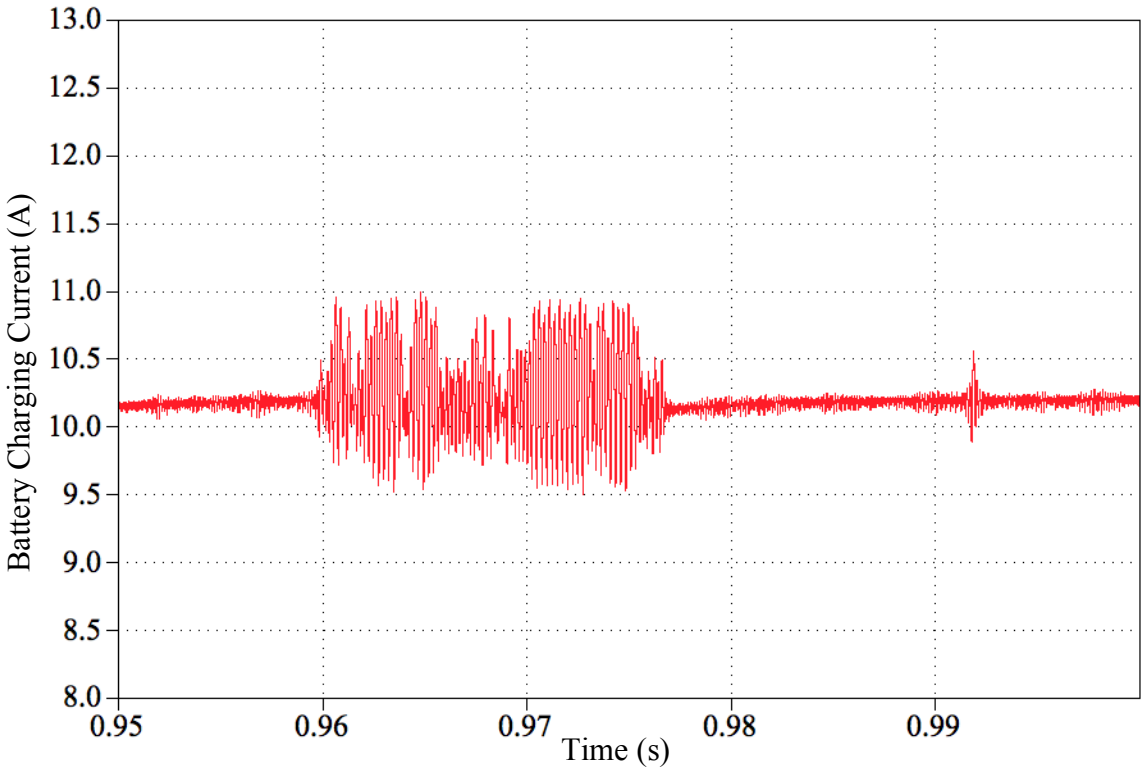


Figure 4.12: Receiver controlled model battery ripple current (2 kW test).

Large currents at the utility connection can be found in the simulation. These are the result of high reactive power demands due to the filtering capacitor on the receiver and the method by which power control is performed. Unneeded energy transferred to the receiver is blocked by the buck-boost converter and built up in the capacitor. As the voltage builds on the filtering capacitor, the converter's ability to limit the current is compromised due to limitations on switching frequency. When less voltage is on the capacitor, the ripple current into the battery is significantly reduced.

A second simulation was performed at 25 kHz at a requested load power of 4 kW and a coupling coefficient of 0.3. Again, Figure 4.13 shows the grid connected voltage and current prior to power factor correction, while Figure 4.14 shows that the PFC was able to bring the system near to unity displacement power factor with low THD (3.3 %).

Again, large currents were present in the system due to the method of power control. The system was further tested over a variety of conditions with different coupling coefficients, operational frequencies, and power requests. These results can be seen in Table 6. All results show a high power factor while maintaining a low THD. Significant increases in efficiency can be noted when the system is operating near the minimum reactive power frequencies and at higher coupling coefficients.

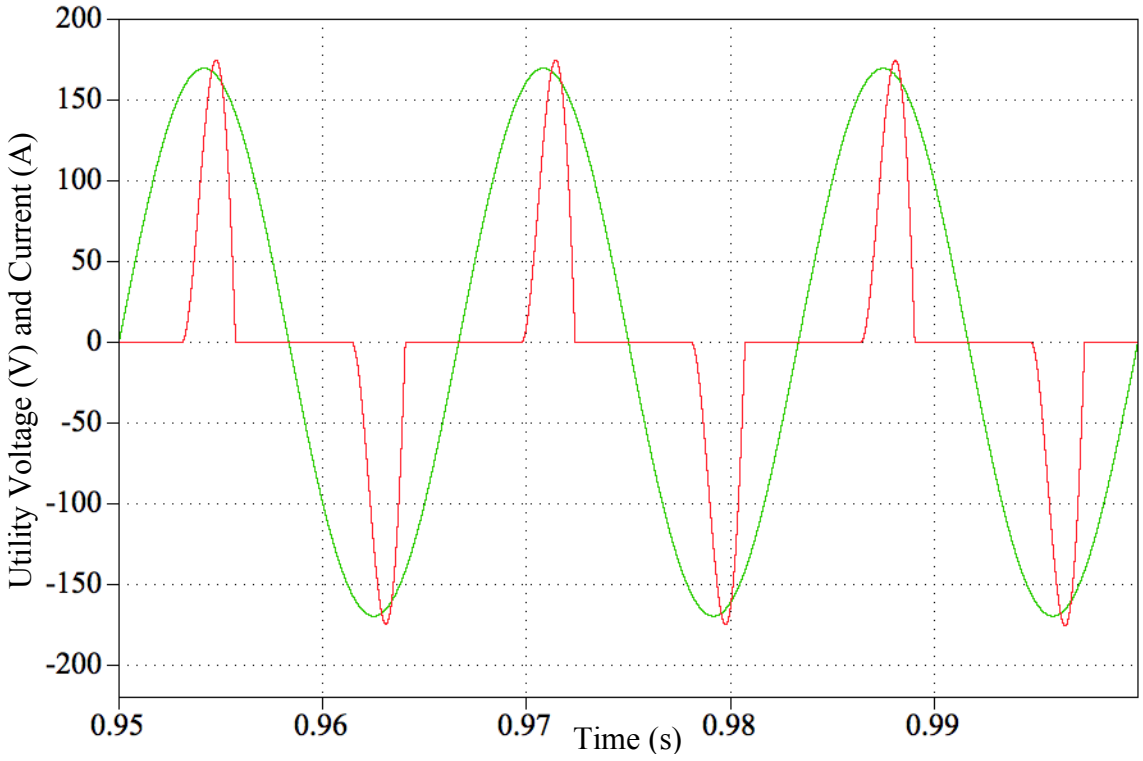


Figure 4.13: Receiver controlled system without PFC (4kW test).

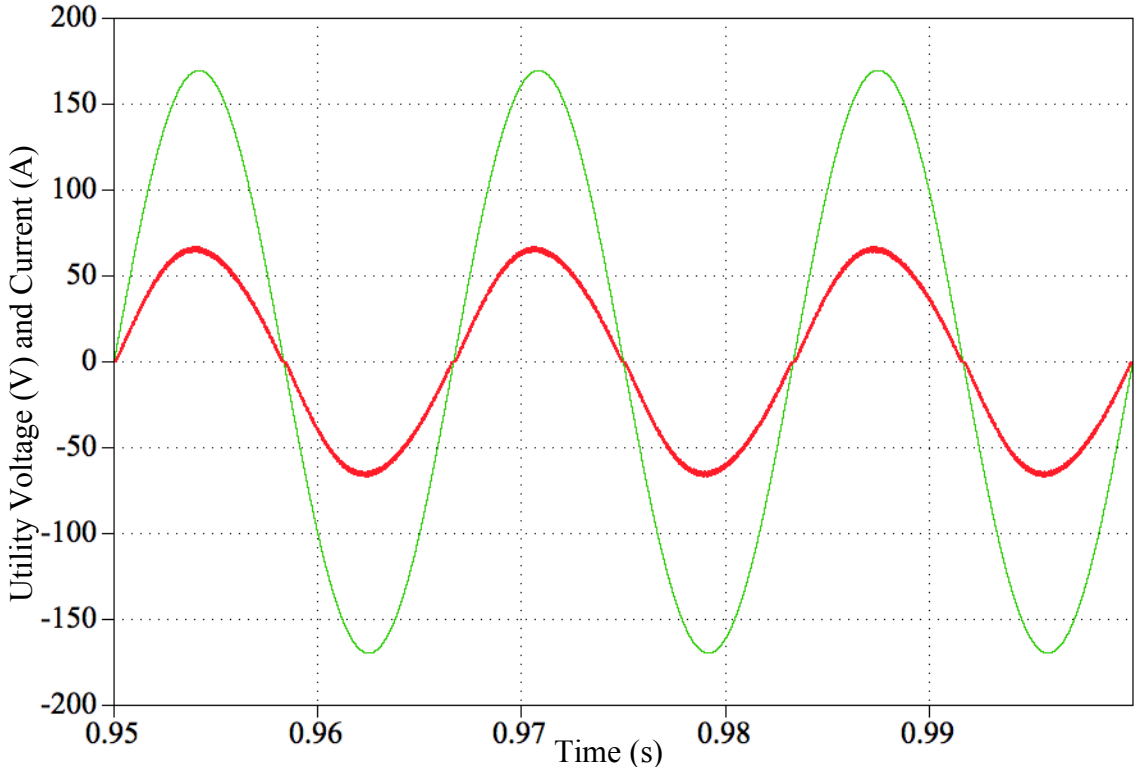


Figure 4.14: Receiver controlled model utility voltage and currents (4 kW test).

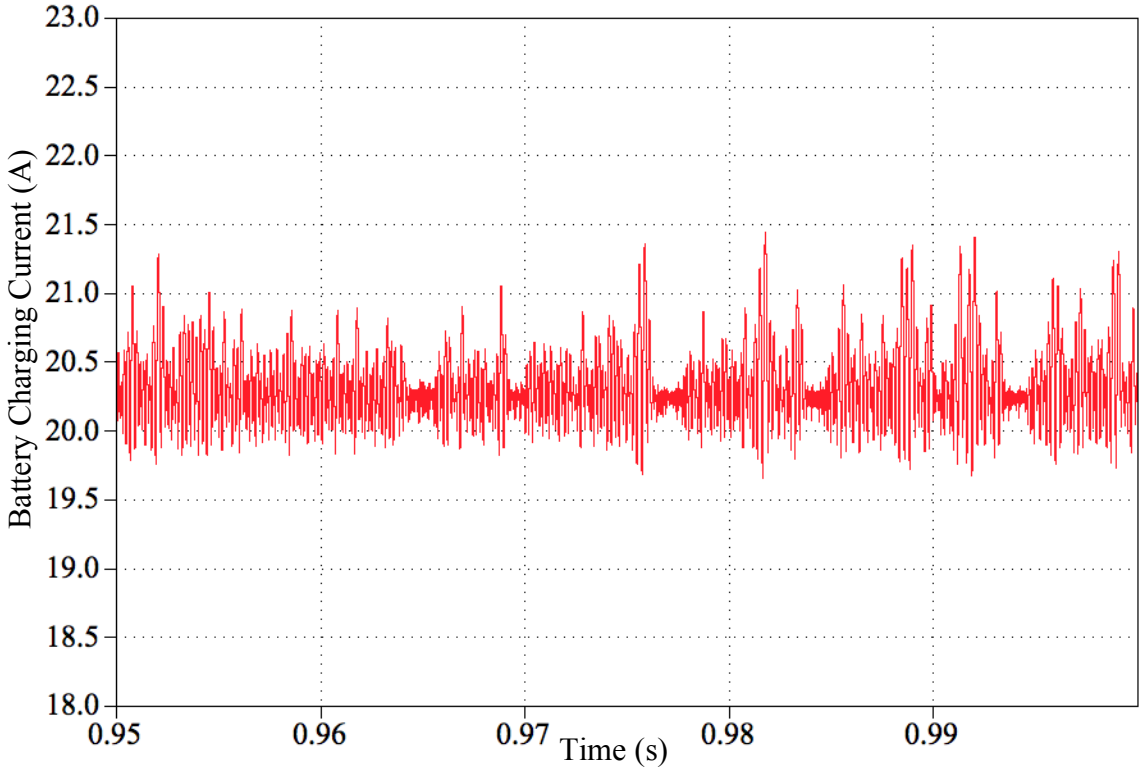


Figure 4.15: Receiver controlled model battery ripple current (4 kW test).

Table 6: Simulation results for the receiver controlled system

k	Operational Frequency	Output Power	Input Power	Efficiency	THD	Power Factor	Battery I_{ripple}
0.15	f_0 = 20 kHz	2 kW	3.6 kW	55.2 %	3.9 %	1	0.87 A
		4 kW	5.2 kW	77.0 %	3.3 %	1	0.86 A
	f_0 = 23 kHz	2 kW	4.1 kW	49.4 %	3.4 %	1	0.77 A
		4 kW	6.2 kW	64.6 %	2.8 %	1	0.80 A
	f_0 = 25 kHz	2 kW	12 kW	17.9 %	2.9 %	1	1.05 A
		4 kW	13 kW	32.1 %	2.9 %	1	0.96 A
0.3	f_0 = 20 kHz	2 kW	20 kW	11.8 %	3.1 %	1	2.22 A
		4 kW	22 kW	19.8 %	3.0 %	1	2.30 A
	f_0 = 23 kHz	2 kW	2.5 kW	80.0 %	5.4 %	1	0.55 A
		4 kW	4.6 kW	87.2 %	3.6 %	1	0.54 A
	f_0 = 25 kHz	2 kW	3.3 kW	60.2 %	4.2 %	1	0.86 A
		4 kW	5.5 kW	72.6 %	2.9 %	1	0.87 A
0.4	f_0 = 20 kHz	2 kW	3.4 kW	59.5 %	4.4 %	1	0.68 A
		4 kW	5.1 kW	78.3 %	3.6 %	1	0.82 A
	f_0 = 23 kHz	2 kW	2.3 kW	87.7 %	5.1 %	1	0.04 A
		4 kW	4.4 kW	91.2 %	3.5 %	1	0.04 A
	f_0 = 25 kHz	2 kW	2.5 kW	81.4 %	4.8 %	1	0.42 A
		4 kW	4.6 kW	87.3 %	3.3 %	1	0.06 A
	f_0 = 28 kHz	2 kW	7.4 kW	27.7 %	3.1 %	1	0.81 A
		4 kW	9.8 kW	41.2 %	2.8 %	1	0.84 A

The range of frequencies for simulations was selected based on the viable operating frequencies at each coupling coefficient. Since the efficiency was relatively high during the 25 kHz tests for a coupling coefficient of 0.4 and because the band of potential operating frequencies was shown to be wider in Chapter 2, the 0.4 coupling coefficient can be seen tested at 28 kHz.

Specific interest should be given to the highlighted rows. When the system is operating near its resonant point, the efficiency is significantly increased over non-

resonant frequencies. The frequencies surrounding the resonant point were selected to show the range of frequencies that are able to transmit power. Similar to the analysis performed in Chapter 2, higher coupling coefficients are more likely to have a range of operating frequencies where high efficiency can be obtained. This will allow the inverter the option to select an operating frequency that has minimum reactive power, while still providing high efficiency.

This first set of simulations reveals that the power factor correction method is sufficient and provides a low THD load characteristic to the utility. Unfortunately, this model yields low efficiencies at most tested operating points. A second model has been designed in the next section to increase system efficiency while still maintaining a high power factor.

4.3 Transmitter Controlled System Simulation

Now that the operation of the system has been established, a second control method will be implemented to improve the overall efficiency and reduce the amount of components on the receiver. This round of simulations demonstrates the use of the controls within the inverter to reduce the reactive power at the transfer system by adjusting the operational frequency. While this method can prove useful, it requires that the transmitter be in contact with the receiver. The amount of power transferred will be set by controlling the magnitude of the quasi-square wave by moving the previously designed buck-boost converter to the transmitter and limiting it to buck operation. Retaining the buck-boost converter can also allow it to be used as an active filter to reduce the 60 Hz harmonics from the inverter input voltage. A block diagram of this system can be seen in Figure 4.16.

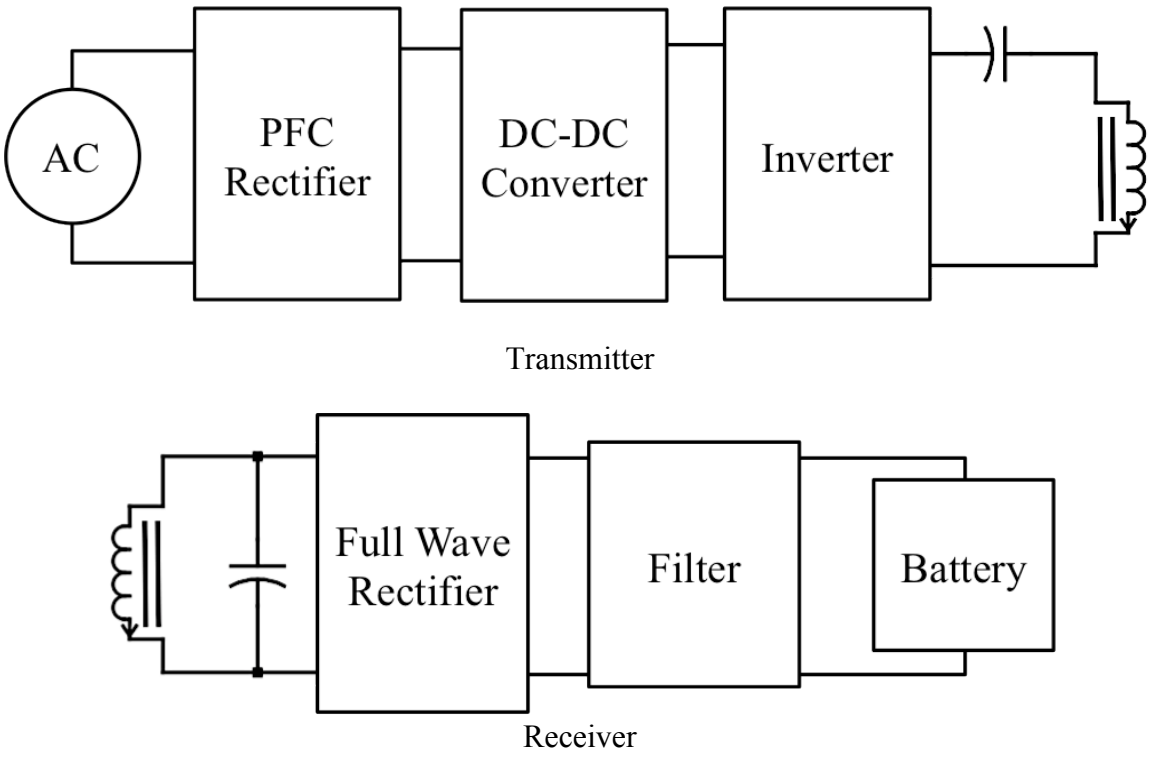


Figure 4.16: Transmitter controlled system block diagram

The first round of simulations was performed at 23 kHz at a requested load power of 2 kW and a coupling coefficient of 0.15. Similar to above, Figure 4.17 reveals the grid connections before power factor correction was implemented. Figure 4.18 shows that the PFC was still able to bring the system near to unity power factor with a THD of 4.6 %. The simulation also revealed a decrease in necessary input power by over 900 W due to the change to transmitter power control, while maintaining the 2 kW power request seen in Figure 4.19. This input power decrease lead to an overall system efficiency of 76.6 % (up from 55.2 %).

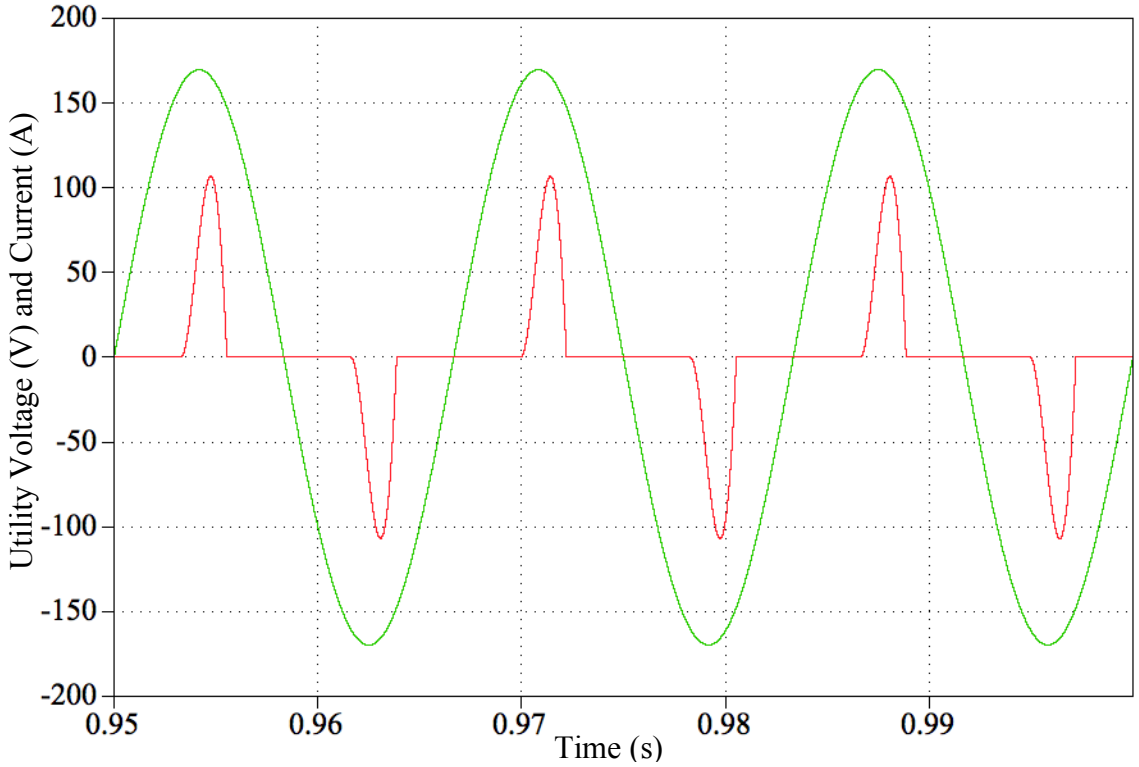


Figure 4.17: Transmitter controlled system without PFC (2kW test).

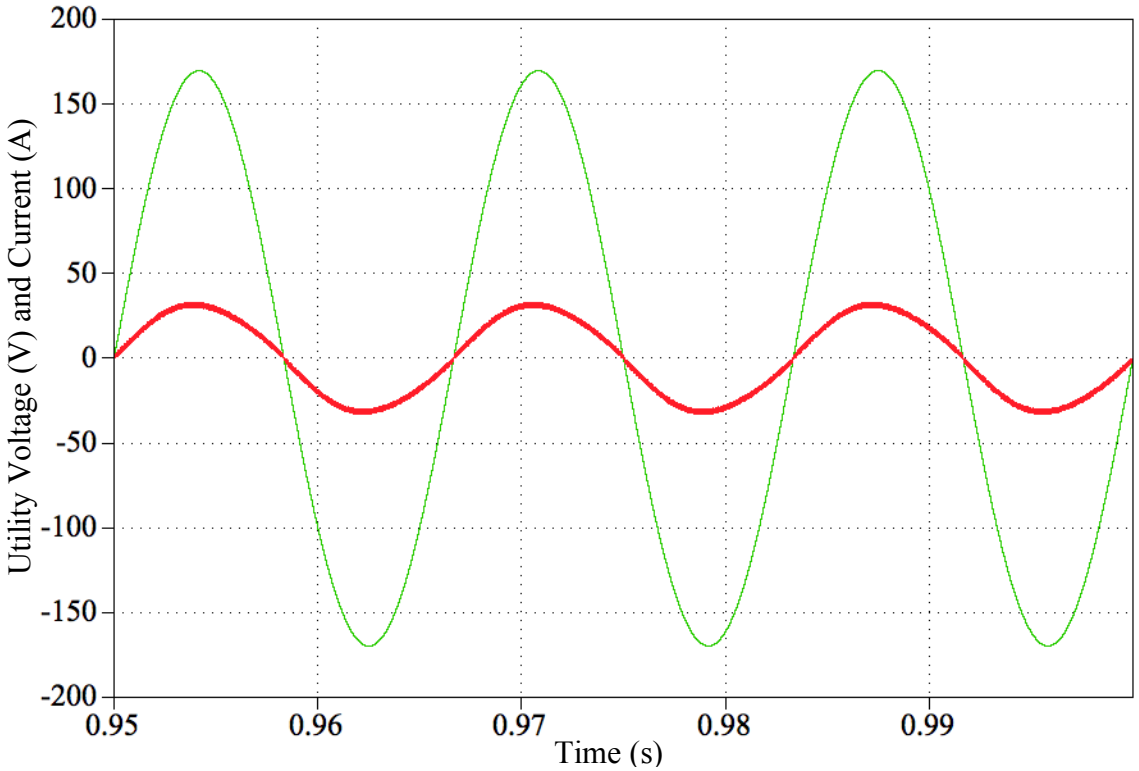


Figure 4.18: Transmitter controlled model utility voltage and currents (2 kW test).

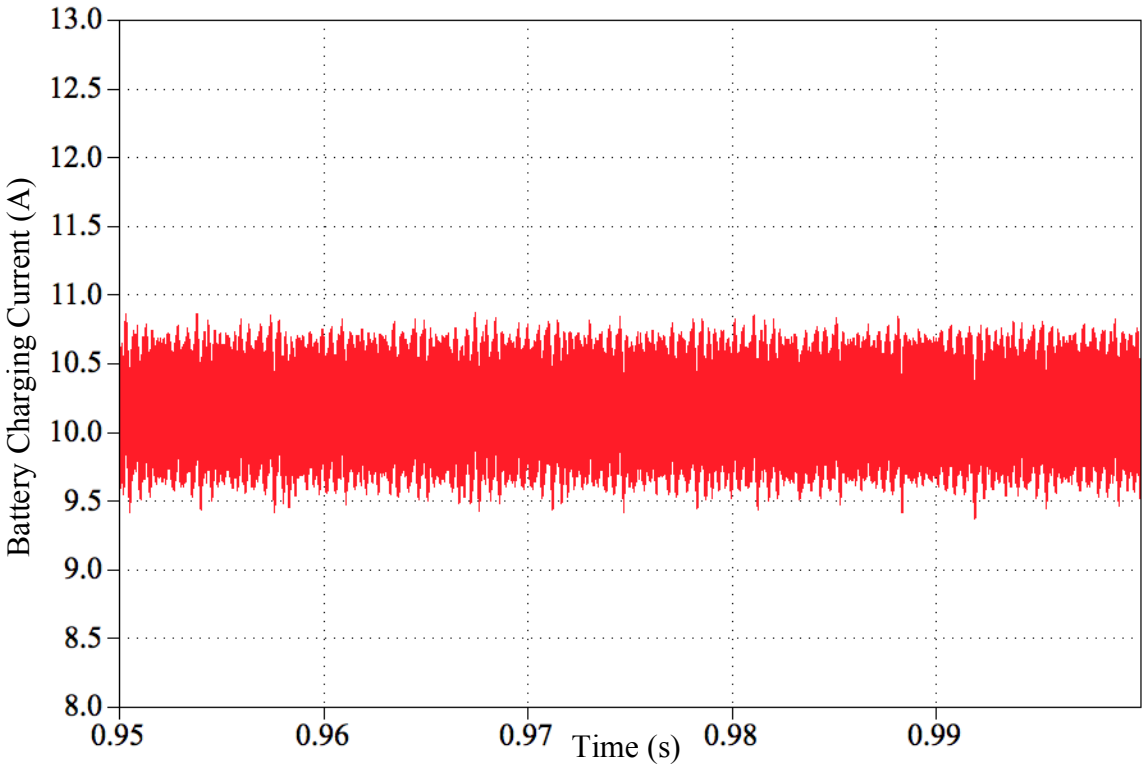


Figure 4.19: Transmitter controlled model battery ripple current (2 kW test).

The second simulation to be discussed was run at 25 kHz at a requested power load of 4 kW and a coupling coefficient of 0.3. Figure 4.20 shows the utility connections prior to adding the power factor correction scheme, while Figure 4.21 reveals that the power factor correction device was able to bring the displacement power factor to near unity and have low THD (3.8 %). The battery charging voltage and current can be seen in Figure 4.22. This model shows a decrease in input power of approximately 370 W from the previous simulation model, improving overall system efficiency to 79.1 % from 72.6 %.

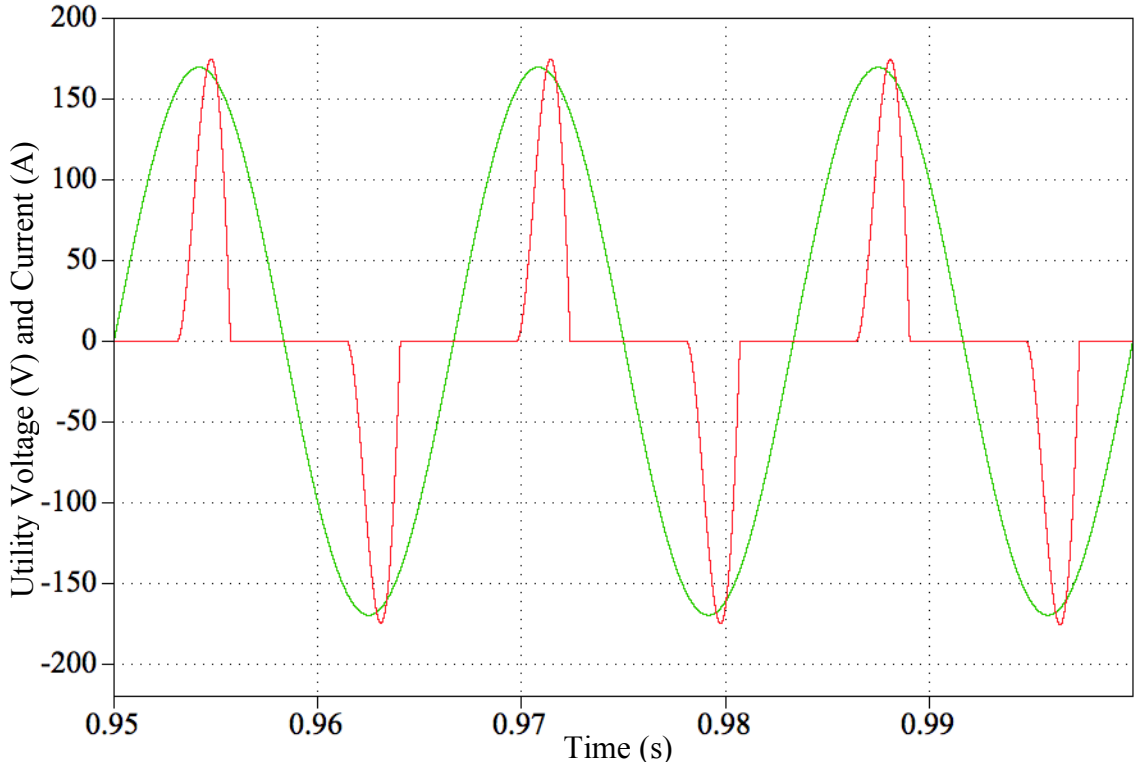


Figure 4.20: Transmitter controlled system without PFC (4kW test).

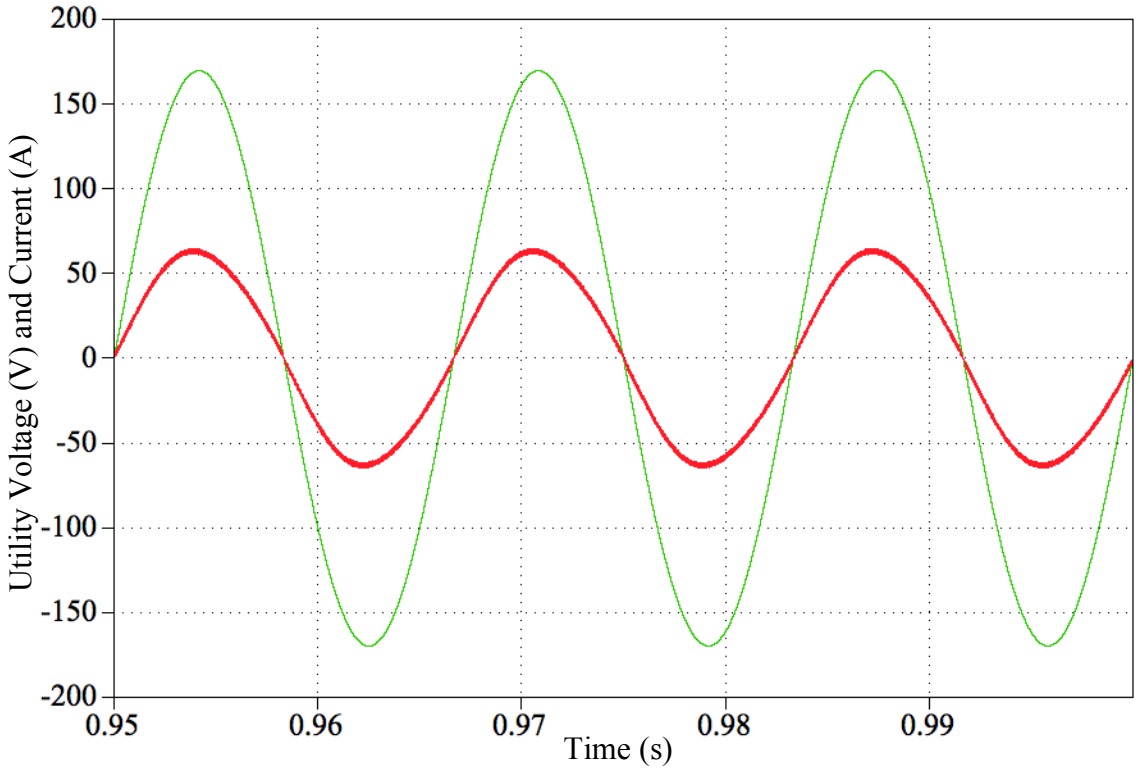


Figure 4.21: Transmitter controlled model utility voltage and currents (4 kW test).

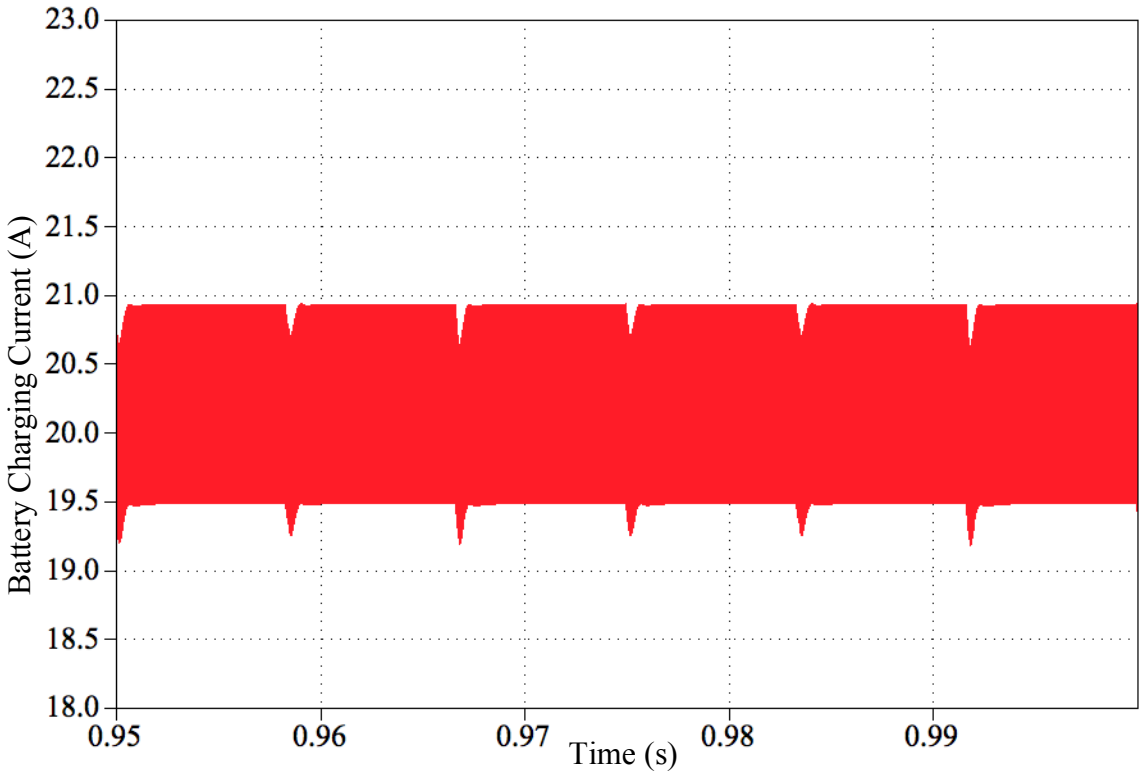


Figure 4.22: Transmitter controlled model battery ripple current (4 kW test).

This system was also simulated over a variety of conditions. Results from these simulations can be seen in Table 7. All results show a low reactive power component at the grid connection and reveal that the system delivers the requested power to the load. Since the buck-boost converter was moved instead of removed completely, it retains its ability to act as an active filter for the 60 Hz harmonics. In contrast with the previous simulations, the previously low system efficiencies have been improved overall. However, moving the buck-boost converter changes the load characteristics of the system.

Table 7: Simulation results for the transmitter controlled system

k	Operational Frequency	Output Power	Input Power	Efficiency	THD	Power Factor	Battery I_{ripple}
0.15	f_0 = 20 kHz	2 kW	2.7 kW	76.6 %	4.6 %	1	0.71 A
		4 kW	5.9 kW	67.8 %	3.3 %	1	1.16 A
	f_0 = 23 kHz	2 kW	3.0 kW	70.4 %	5.0 %	1	0.74 A
		4 kW	6.8 kW	60.8 %	3.3 %	1	0.86 A
	f_0 = 25 kHz	2 kW	3.5 kW	59.3 %	4.5 %	1	0.51 A
		4 kW	7.6 kW	53.3 %	2.9 %	1	0.78 A
0.3	f_0 = 20 kHz	2 kW	2.3 kW	89.6 %	5.9 %	1	0.68 A
		4 kW	4.5 kW	89.3 %	3.9 %	1	0.83 A
	f_0 = 23 kHz	2 kW	2.4 kW	87.5 %	5.7 %	1	0.69 A
		4 kW	4.8 kW	84.2 %	3.9 %	1	0.98 A
	f_0 = 25 kHz	2 kW	2.5 kW	83.0 %	5.6 %	1	0.63 A
		4 kW	5.4 kW	79.1 %	3.6 %	1	0.88 A
0.4	f_0 = 20 kHz	2 kW	2.2 kW	92.5 %	6.2 %	1	0.78 A
		4 kW	4.5 kW	91.3 %	3.9 %	1	1.14 A
	f_0 = 23 kHz	2 kW	2.3 kW	90.8 %	5.9 %	1	0.59 A
		4 kW	4.7 kW	88.9 %	3.8 %	1	0.92 A
	f_0 = 25 kHz	2 kW	2.3 kW	87.8 %	6.0 %	1	0.63 A
		4 kW	4.7 kW	87.1 %	3.8 %	1	0.93 A
	f_0 = 28 kHz	2 kW	2.5 kW	82.3 %	4.9 %	1	0.43 A
		4 kW	4.9 kW	82.2 %	3.4 %	1	0.76 A

When the buck-boost converter was moved, the real and reactive power transfer characteristics of the system changed as well. This accounts for the peak efficiency differences between Table 6 and Table 7 with regards to coupling coefficients and operational frequencies. However, overall system efficiencies improved because less power was expended in the transfer system as the DC link capacitor on the receiver was charging.

Similar to the previous model's simulation results, higher coupling coefficients reveal a larger frequency range at which highly efficient power is transferred. These efficiencies are centered at lower frequencies due to the change in the load model. This is because the load characteristics have been altered in placing the buck-boost converter on the transmitter rather than the receiver, supporting the results of testing earlier in the chapter.

4.4 Simulation Summary

This chapter has detailed the steps taken in creating a model that accurately represents two potential WPT systems. An equivalent circuit for a WPT system was developed that closely models an experimental system used at ORNL. Other major components, including a high frequency inverter, a buck-boost DC-DC converter, and a PFC were also developed.

After the models were constructed, tests were run to compare the operation of two possible systems. While both system models were able to perform power factor correction, each had its strengths and weaknesses. The first set of simulations featured a receiver controlled system that was able to operate without the need for communication between the transmitter and receiver. However, the second simulated model was transmitter controlled and was able to operate more efficiently. The second model also contained fewer components on the receiver, making it a more practical choice for automotive manufacturers.

Chapter 5 Conclusions and Recommendations

5.1 Conclusions

From the simulations presented in this thesis, it can be concluded that wireless power transfer systems can be highly efficient and operate near unity power factor if measures are taken to closely control the operating frequency and voltage levels throughout the system. An extensive overview of the physical operation of WPT systems has been established in Chapter 2, followed by highlights of the research being performed to make improvements to the technology.

A model for an experimental WPT system was developed in Chapter 4, along with several major components that may be found in an electric vehicle application. The components were arranged in two different configurations. The results of the simulations were then compared. Of primary interest to this thesis, both systems showed a unity power factor for all simulations, proving that WPT systems can have unity power factor at the grid connections.

The targets of this thesis have been to reveal the most current information on the operation of WPT systems and address the possibility of poor power factor at the grid connection. The first goal was reached with an extensive exploration into the workings of the system. By using a power factor correction device at the grid connection, the goal of power factor correction was realized in simulation. A method of reactive power reduction was also explored within the high frequency inverter and transfer system to improve system efficiency.

5.2 Recommendations

One recommendation that could be made would be to examine the communication channel that must be developed to make WPT possible. This will be a more demanding issue when performing in-motion charging. One of the largest challenges will be to find a method to determine location without relying on a communication system to eliminate the possibility of latency. Since transfer systems are affected by vertical and lateral displacement, the challenge will not be simple to overcome.

It may prove useful to use an active rectifier for the power factor correction device. Not only does this inherently provide voltage reduction capabilities that proved useful in the second set of simulations, but it will also be more useful for integration into a three-phase system. However, as stated earlier, it will require an input filter.

References

[1] "Fuel Economy: Where the Energy Goes." [Online]. Available: http://www.fueleconomy.gov/feg/atv.shtml [Accessed: 12-Jun-2012].

[2] Rogers, S., "Advanced Power Electronics and Electric Motors (APEEM) R&D Program Overview." [Online]. Available: http://www1.eere.energy.gov/vehiclesandfuels/pdfs/merit_review_2011/adv_power_electronics/ape00a_rogers_2011_o.pdf [Accessed: 2-Jun-2012].

[3] "2012 Toyota Camry Hybrid." [Online]. Available: http://usnews.rankingsandreviews.com/cars-trucks/Toyota_Camry-Hybrid/2012/specs/Camry-Hybrid-4dr-Sdn-XLE-(Natl)-334775/ [Accessed: 24-Jun-2012].

[4] "2012 Toyota Camry." [Online]. Available: http://www.leftlanenews.com/new-car-buying/toyota/camry/specifications/ [Accessed: 24-Jun-2012].

[5] "Hybrid Electric Vehicles." [Online]. Available: http://www.afdc.energy.gov/afdc/vehicles/electric_basics_hev.html [Accessed: 15-Jun-2012].

[6] "Series-Parallel Hybrid Cars." [Online]. Available: http://1st-in-hybrid.com/series-hybrid/ [Accessed: 15-Jun-2012].

[7] "Toyota Prius- Power Split Device (PSD)." [Online]. Available: http://eahart.com/prius/psd/ [Accessed: 17-Jun-2012].

[8] "Inductive Charging Technology." [Online]. Available: http://www.utc.edu/Academic/EngineeringProjects/SmartCart/UTCEngineeringProjects-Technologies.php [Accessed: 19-Jun-2012].

[9] J. Miller, Personal Conversation.

[10] K. Fotopoulou, B. W. Flynn, "Wireless Power Transfer in Loosely Coupled Links: Coil Misalignment Model," IEEE Transactions on Magnetics, vol. 47, no. 2, pp. 416-430, Feb. 2011.

[11] M. Budhia, G. A. Covic, J. T. Boys, "A new IPT magnetic coupler for electric vehicle charging systems," IEEE Industrial Electronics Society Conference, 7-10 Nov. 2010, pp. 2487-2492.

[12] M. Budhia, G. A. Covic, J. T. Boys, "Design and Optimization of Circular Magnetic Structures for Lumped Inductive Power Transfer Systems," IEEE Transactions on Power Electronics, vol. 26, no. 11, pp. 3096-3108, Nov. 2011.

[13] M. Budhia, G. A. Covic, J. T. Boys, C. Y. Huang, "Development and evaluation of single sided flux couplers for contactless electric vehicle charging," IEEE Energy Conversion Congress and Exposition (ECCE), 17-22 Sept. 2011, pp. 614-621.

[14] N. Oodachi, K. Ogawa, H. Kudo, H. Shoki, S. Obayashi, T. Morooka, "Efficiency improvement of wireless power transfer via magnetic resonance using transmission coil array," IEEE International Symposium on Antennas and Propagation (APSURSI), 3-8 July 2011, pp. 1707-1710.

[15] H. Hao, G. Covic, M. Kissin, J. Boys, “A parallel topology for inductive power transfer power supplies,” IEEE Applied Power Electronics Conference and Exposition (APEC), 6-11 March 2011, pp. 2027-2034.

[16] Budhia, M.; Covic, G.A.; Boys, J.T.; Chang-Yu Huang; , “Development and evaluation of single sided flux couplers for contactless electric vehicle charging,” IEEE Energy Conversion Congress and Exposition (ECCE), 17-22 Sept. 2011, pp. 614-621.

[17] J. Huh, W. Lee, G. Cho, B. Lee, C. Rim, “Characterization of novel Inductive Power Transfer Systems for On-Line Electric Vehicles,” IEEE Applied Power Electronics Conference and Exposition (APEC), 6-11 March 2011, pp. 1975-1979.

[18] S. Raabe, J. T. Boys, G. A. Covic, “A high power coaxial inductive power transfer pickup,” IEEE in Power Electronics Specialists Conference (PESC), 15-19 June 2008, pp. 4320-4325.

[19] Seungyoung Ahn; Joungho Kim, “Magnetic field design for high efficient and low EMF wireless power transfer in on-line electric vehicle,” Proceedings of the 5th European Conference on Antennas and Propagation (EUCAP), 11-15 April 2011, pp. 3979-3982.

[20] J. T. Boys, C. Y. Huang, G. A. Covic, “Single-phase unity power-factor inductive power transfer system,” IEEE Power Electronics Specialists Conference, 15-19 June 2008, pp. 3701-3706.

[21] Y. H. Chao, J. J. Shieh, C. T. Pan, W. C. Shen, “A Closed-form Oriented Compensator Analysis for Series-parallel Loosely Coupled Inductive Power Transfer Systems,” IEEE Power Electronics Specialists Conference, 17-21 June 2007, pp. 1215-1220.

[22] M. G. Egan, D. L. O'Sullivan, J. G. Hayes, M. J. Willers, C. P. Henze, “Power-Factor-Corrected Single-Stage Inductive Charger for Electric Vehicle Batteries,” IEEE Transactions on Industrial Electronics, vol. 54, no. 2, pp. 1217-1226, April 2007.

[23] N. A. Keeling, G. A. Covic, J. T. Boys, “A Unity-Power-Factor IPT Pickup for High-Power Applications,” IEEE Transactions on Industrial Electronics, vol. 57, no. 2, pp. 744-751, Feb. 2010.

[24] R. W. Erickson, D. Maksimovic, “Converter Circuits,” in *Fundamentals of Power Electronics*, 2nd ed., Secaucus, Kluewr Acedemic, 2000, ch. 6, sec. 2, pp. 131-184.

[25] “Power Factor Correction,” [Online]. Available: http://www.schockpower.com/pfc.htm [Accesseed: 20-Feb-2012].

[26] P. N. Ekemezie, "Design of a power factor correction ac-dc converter," AFRICON 2007, pp. 1-8, 26-28 Sept. 2007.

[27] M. Pickelsimer, L. Tolbert, B. Ozpineci, J. M. Miller, “Simulation of a wireless power transfer system for electric vehicles with power factor correction,” IEEE International Electric Vehicle Conference (IEVC), 4-8 March 2012, pp. 1-6.

Vita

Michael Christopher Pickelsimer was born in Cleveland, Tennessee. He graduated from Walker Valley High School in 2007. Later, Michael went on to receive his Bachelor's of Science degree in Electrical Engineering from The University of Tennessee, Knoxville in 2011. Michael then continued on to graduate studies at The University of Tennessee, Knoxville, where he graduated in August 2012 with his Master's of Science degree in Electrical Engineering. He plans to have a career with which he may assist with the advancement of electric vehicles.